This is to certify that the

thesis entitled

CHARACTERIZATION OF COMPOSITES BY INTERNAL FRICTION

AND ELASTIC MODULUS MEASUREMENTS

presented by

WON JAE LEE

has been accepted towards fulfillment
of the requirements for

MASTERS degree in MATERIALS SCIENCE

Eldon D. Case

E. D. CASE

Major professor

Date Feb 22, 1988

CHARACTERIZATION OF COMPOSITES BY INTERNAL FRICTION AND ELASTIC MODULUS MEASUREMENTS

By

Won Jae Lee

A THESIS

Submitted to

Michigan State University

in partial fulfillment of the requirements

for the degree of

MASTER OF SCIENCE

Department of Metallurgy, Mechanics and Material Science

1988

ABSTRACT

CHARACTERIZATION OF COMPOSITES BY INTERNAL FRICTION AND ELASTIC MODULUS MEASUREMENTS

By

Won Jae Lee

Internal friction and Young's modulus were studied on polymer composites and SiC whisker/alumina composites using the sonic resonance technique. Polymer composites reinforced with unidirectional fibers exhibit modulus and internal friction anisotropy. Usually, elastic modulus and internal friction showed a inverse relationship. The internal friction increased with decreasing interfacial shear strength. For the SiC whisker reinforced alumina composites, microcracks introduced by water quenching were detected by internal friction and Young's modulus measurements. As thermal shock progresses, Young's modulus decreases and internal friction increases. A quantitative relation between the modulus and internal friction is developed. Elevated Young's modulus and internal friction also were investigated for the SiC whisker reinfored alumina composite.

ACKNOWLEDGEMENTS

First and formost, I would like to thank my adviser, Professor E. D. Case for his help and support over the course of this investigation. Special thanks are given to D. Bray, Alcoa, for providing the SiC whisker/alumina composites. Special thanks are also given to M. Rich and Professor L. Drzal for providing the polymer composites.

I would like also acknowledge the support of the Research Excellence Economic Development Fund, State of Michigan, and of the National Science Foundation through grant number MSM-8706915.

I would like to thank my mother and father for their endless love and help over my entire life. Also I would like to thank my wife Haesun for her endless love.

TABLE OF CONTENTS

LIST OF TABLES

LIST OF FIGURES

1. INTRODUCTION

Most ceramic materials are susceptible to failure under mechanical or thermal loadings. Fiber and whisker reinforcement of a number of ceramic matrix composite materials have provided drastic improvements in the strength and fracture properties, especially at elevated temperature. Tai-il Mah et al. [1] recently reviewed developments in fiber-reinforced ceramic composites. Besides the strengthening and toughening of reinforced ceramic composites, the strain-to-failure of some reinforced ceramic composites can be increased by a factor of ten times or more as compared to that of the unreinforced ceramics [2,3].

In composites, there exists either chemical or physical bonds between the fiber and the matrix. For fiber reinforced ceramic composites, the interfacial bonding between the fiber and the matrix can affect the strain-to-failure curve. Bonding between the fiber and matrix that is too strong may cause brittle fracture, but proper bonding can cause a considerable increase in strain to failure, by the mechanism of fiber pull out. When the bonding between fibers and matrix is not sufficiently strong, the fibers can debond and slip within the matrix before the composite failure. The mechanism of fiber pull out results in the relatively high strain [4].

An incomplete understanding of the nature of the interfacial bonding can be attributed, at least in part, to the lack of nondestructive techniques to characterize the interfacial bonding. Disruption of interfacial bonding occur due to interfacial shear stresses that result from slippage between the matrix and the fiber. Thus the relative slip between the fiber and the matrix is important in assessing the nature of interfacial bonding in a composite.

It is proposed that the fiber-matrix friction in ceramic composites be studied nondestructively by internal friction and elasticity techniques. The increase in internal friction observed to accompany microcracking in brittle materials has been explained in terms of rubbing of opposing faces of the microcrack [5]. As the material sonically vibrates, the opposite surfaces of the microcracks rub against each other, resulting in a frictional impedence (increasing in internal friction). A similar dependence may exist for the internal friction changes as a function of the relative slip, or rubbing, of the matrix and embedded fibers in a composite.

Thus, internal friction and elastic modulus measurements by sonic methods are nondestructive. In addition, both internal friction and elastic modulus of ceramics are thought to be very sensitive to the microstructural changes [5-10]. For example, the elastic moduli and internal friction are sensitive to phase

changes [10], microcracking [5,7,9], porosity [8], and grain boundary sliding [5,6]. Elasticity and internal friction can thus provide important information on the interfacial bonding and the microstructural stability of the ceramic composites.

Internal friction values for numbers of metals, glasses, and polymers can be found in the literature [11,12]. However, little data has been reported for the internal friction of ceramics, especially ceramic composites.

In the present study, internal friction and elastic modulus of the fiber-reinforced polymer and whisker-reinforced ceramic were measured using the flexural resonance method. The effects of interfacial bonding and thermal shock upon the internal friction and elastic modulus of the materials were also investigated.

2. BACKGROUND

2-1. Fundamentals of Methods for Measuring Internal Friction

Damping effect within the solid is internal friction. Anelasticity or internal friction of solids is one of the important properties which are indirectly related to their elastic moduli. Let us consider briefly the relationship among the various measures of internal friction.

Generally, the method of measuring internal friction of solids can be divided into four categories.[13]:

1. direct observation of stress-strain curve
2. free-vibration method (logarithmic decrement)
3. forced-vibration method (full width half maxima)
4. wave propagation method

The definition of mechanical damping, as the ratio $\Delta E/E$ between the energy ΔE dissipated during one stress cycle and the maximal elastic energy E stored in the specimen, suggests one direct way for its measurement. If ΔE is sufficiently large, a measureable rise in the specimen temperature may result from energy dissipation. The stored vibration energy E is determined by the maximum applied stress. Obviously, this method is restricted to relatively high stress levels. Another disadvantage applies to a variation of this method, in which one

measures simultaneously the applied stress and the resulting strain. Mechanical damping manifests itself as a stress-strain hysterisis loop, and is proportional to the area of this loop.

Lower values of the internal friction (order of 10^{-4} or larger) are more commonly measured by a resonance method. The free vibration method which is the oldest and still most popular method is based on the measurement of the decay in amplitude of vibrations during "free vibration." The natural logarithmic of this ratio is commonly called "logarithmic decrement." Figure 1 shows the vibration behavior during free decay. It is defined as follows

$$\delta = [\ln(A/B)]/tf \qquad (1)$$
$$\approx \Delta E/2E$$

where A and B = amplitude of the first and the last vibration considered
f = frequency of vibration
t = time interval between the two successive vibrations
ΔE = energy loss per cycle
E = stored vibration energy.

When the damping is small, the internal friction is expressed by

$$Q^{-1} = \delta/\pi \qquad (2)$$
$$= [\ln(A/B)]/\pi tf.$$

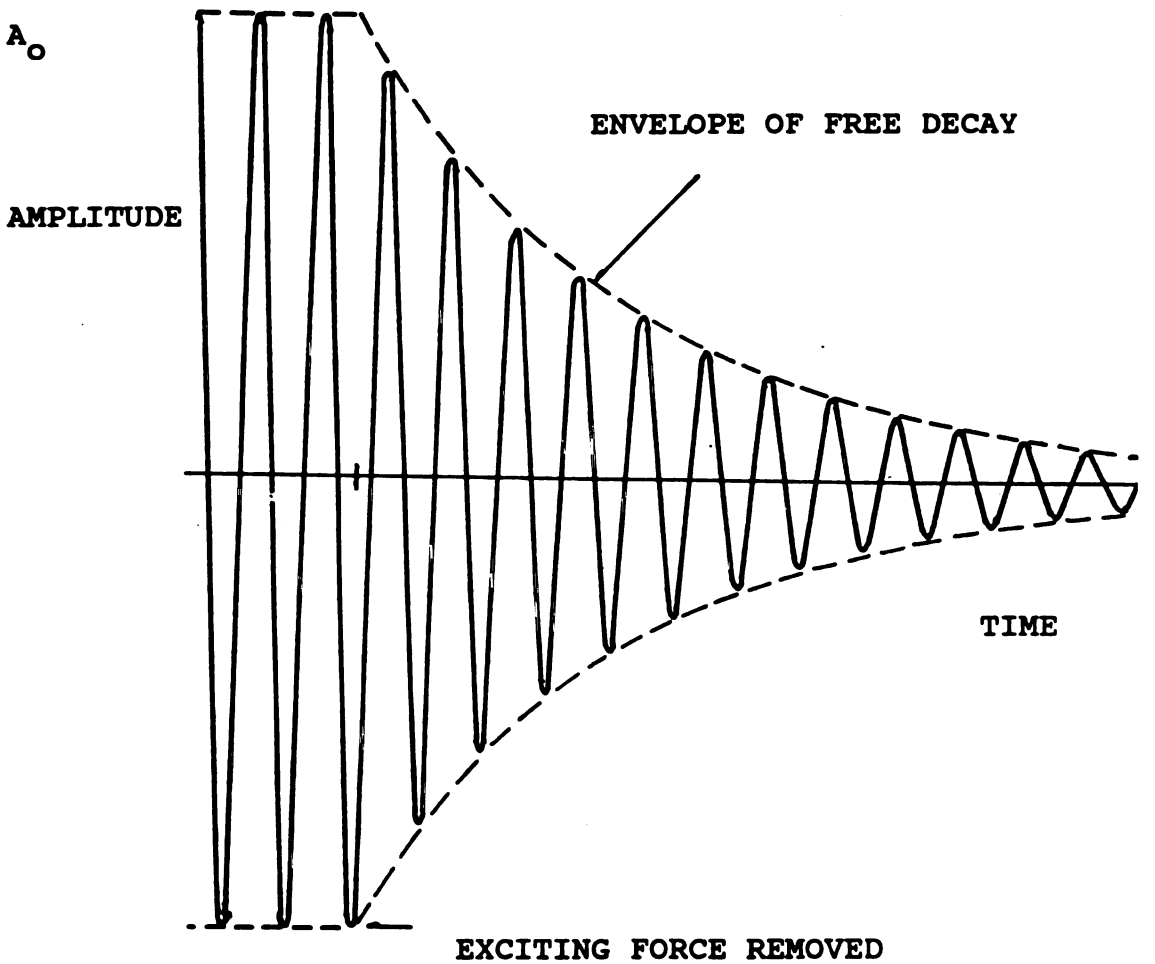

Figure 1. The free decay of natural vibrations of an anelastic solid.

The product, tf, is equal to the number of cycles, N. It may be measured directly by counting the number of cycles during a free decay. As the magnitude of internal friction value decreases, the number of cycles counted during free decay increases. For values of internal friction larger than $1x10^{-3}$, the relatively low number of cycles, N, occuring during the free decay may induce some experimental error. Therefore, this method is effective with specimen having low internal friction values (order of 10^{-4} or higher) and in the case of high frequencies (hundreds Hz to a few hundred kHz) [14].

The standard resonance method can be used as a forced vibration method (full width half maxima). The specimen is forced to vibrate at a certain range of frequencies with constant drive voltage. When the imposed frequency is equal to a resonance frequency of the specimen, the amplitude of vibration reaches a maximum value. If the impressed frequency deviates from the resonance frequency, the amplitude of vibration decreases. Figure 2 shows the resonance peak in the forced vibration. The sharpness of this peak varies inversely with the internal friction. The relative sharpness is readily obtained by

$$\text{relative sharpness} = \Delta f / f_r$$

where Δf = width of the frequency at half maximum amplitude
f_r = resonance frequency.

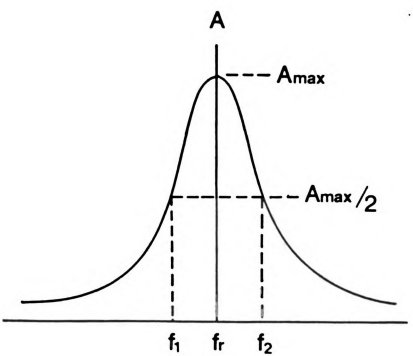

Figure 2. Lorentzian form for the resonance peak in forced vibration.

Zener [15] shows that the ratio, $\Delta f/f_r$, is related to the specific loss in the following relation

$$\Delta f/f_r = \sqrt{3}/2\pi * \Delta E/E \qquad (3)$$
$$= \sqrt{3}/\pi * \delta .$$

Thus the internal friction is expressed as

$$Q^{-1} = \delta/\pi = 0.5773\Delta f/f_r \qquad (4)$$

The forced vibration method is most effective with specimen having values of Δf of several cycles/second. For relatively low damping levels (say $Q^{-1} = 10^{-4}$) a precision of 1 percent for the damping measurement requires a precision of a 10^{-6} in the frequency reading.

Since the attenuation constant of a stress wave through a solid can be related to the internal friction, this provides another method for measuring the internal friction of a specimen. The wave propagation technique consists of determining the amplitude of a stress wave before and after traversing well-known distance. This technique is useful at high frequencies (above several MHz). Using the pulse technique, it is possible to overcome this difficulty. The wave propagation method employs a pulse or wave packet whose length is small compared to the specimen length in the direction of propagation. Figure 3 and figure 4 show the method

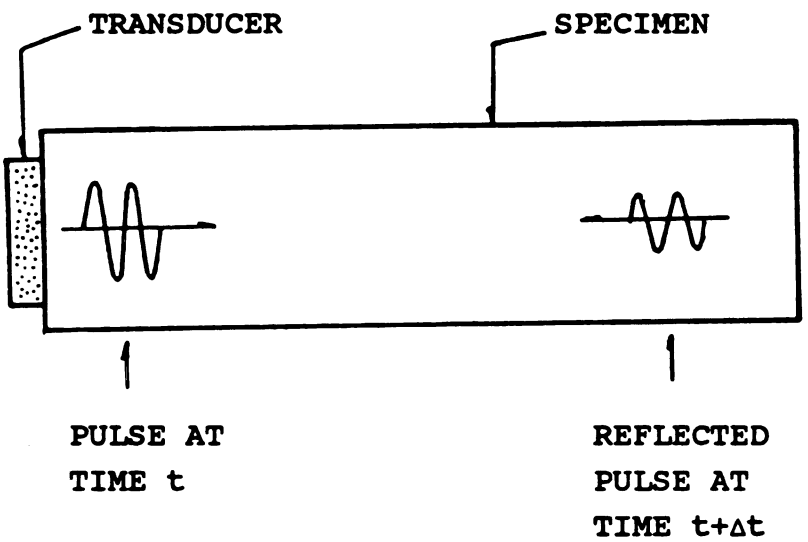

Figure 3. Schematic illustration of ultrasonic pulse method (After Norwick and Berry [13]).

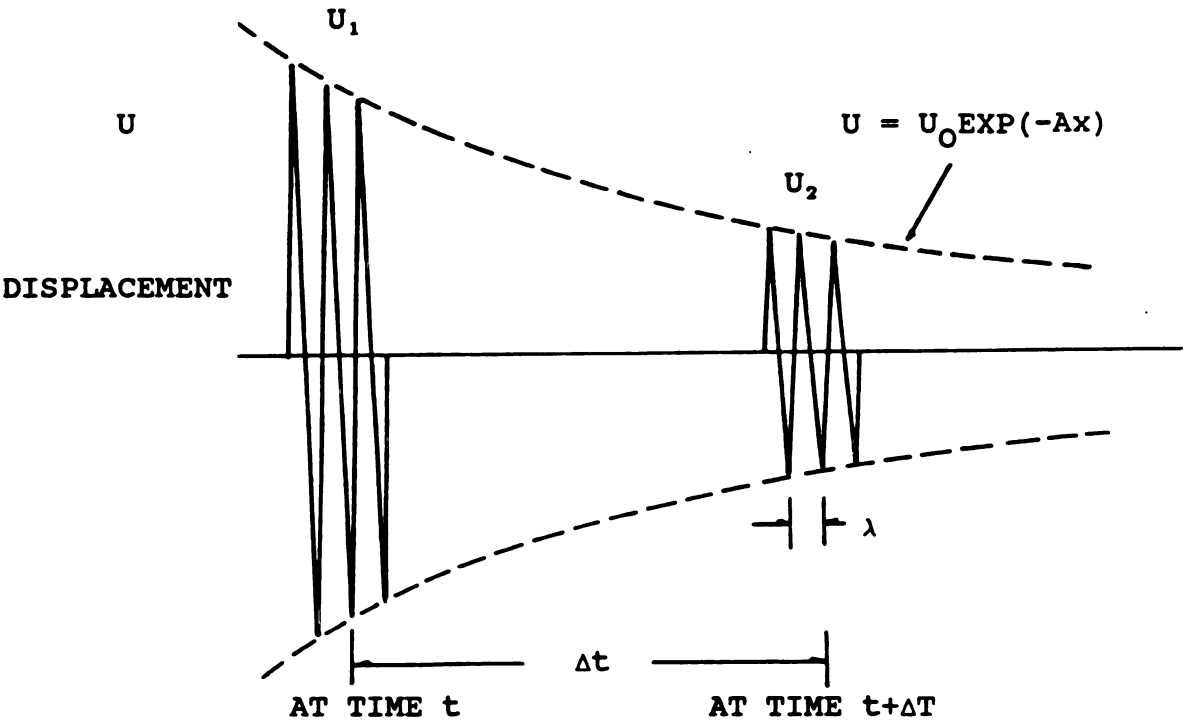

Figure 4. The attenuation of an ultrasonic pulse as it propagates through an anelastic medium.

schematically. A narrow high frequency mechanical pulse is applied to the specimen, and the internal friction is derived from the decrease in amplitude of the wave pulse as it propagates through the specimen. This method may be suitable for materials having much lower values of internal friction than $1x10^{-5}$ [13]. One of the disadvantages of this technique has been that high-temperature effects cannot be investigated due to transducer limitations and difficulties in bonding the transducer to the specimen at high temperature. However, this is being overcome with the developement of high-temperature transducers. Lithium niobate, which can withstand temperatures above 900°C, may provide the means to extend the measurements to high temperatures.

3.EXPERIMENTAL PROCEDURE

3-1. Materials

a) Polymer Composites *

Samples were obtained from the Composite Center at Michigan State University. They were processed in an autoclave for two hours at 75° C. For reasons unknown, they contained a large number of voids. The as-received specimens were initially in the form of scrap plates. They were cut in the shape of prismatic bars by using a Beuhler Isomet cutter employing a diamond wheel. The specimens were held in a grip provided on the diamond cutter. The grip held the specimen by means of two adjustable screws. The dimension of the as-cut specimens is given in table 1. Many characteristics of the samples used for this research are given in table 2.

---

* The polymer composites were given by M. Rich, Composite Center.

Table 1. Dimensions, Mass, and Mass density of Polymer Composite

	Dimensions (cm)	Mass (g)	Mass density (g/cm^3)
AU4 (longitudinal)	9.07x2.45x0.26	8.2429	1.45
(transverse)	7.66x2.42x0.27	6.2280	1.42
AS4 (longitudinal)	7.97x2.46x0.27	7.6392	1.44
(transverse)	7.66x2.42x0.27	7.1050	1.43
AS4C(longitudinal)	7.27x2.41x0.34	8.4674	1.41
(transverse)	9.68x2.44x0.34	11.5600	1.42

Table 2. Characteristics of Polymer Composite

Polymer Composite	Interfacial Shear Strength (Kpsi)*	Interfacial Treatment
AU4	5.4	untreated, unsized
AS4	9.9	surface treated only
AS4C	11.8	surface treated and coated with layer of epoxy

Matrix used: EPON 828 (DGBEA, by Shell)

Fiber used: Polyacrylonitrile based graphite fiber having a diameter of 7.7 microns

* The measurement for this interfacial shear strength was by the uniaxial tension test.

b) Whisker Reinforced Alumina Composites

Whisker reinforced alumina composites used for this research were produced by Alcoa.* The material consists of A-16 SG alumina (a super ground calcined alumina), reinforced with both the Arco and Tokai carbon SiC whiskers. Processing was carried out using pH stabilization in a wet procedure. The material was then dried and hot pressed. The dimension of the as-received specimens is shown in table 3. Table 4 shows some properties of the samples used for this research.

3-2. Room Temperature Elasticity Measurement

The sonic resonance technique described by Forster [16] was used to determine the elastic moduli and internal friction. Figure 5 shows schematically the experimental arrangement used. The modulus equipment measures the resonant frequencies of the specimen. Cotton strings were used to suspend the prismatic specimen horizontally from a driver and a phonograph pickup (Figure 6). An electronic signal produced by a frequency generator (3325A Synthesizer/Function Generator made by Hewlett-Packard)

---

* The whisker reinforced ceramic composites were obtained from D. J. Bray, Technical Superviser, Alcoa Technical Center, Alcoa Center, PA.

Table 3. Dimensions and Mass of Alumina/SiC Composites

	Dimensions (cm^3)	Mass (g)
HP158	7.01x0.702x0.297	5.5893
HP160	7.01x0.700x0.297	5.6291
HP171	7.00x0.700x0.298	5.6039

Table 4. Density and Mechanical Properties of SiC Whisker Reinforced Alumina Composites*

	HP158 (1800°C) A-16SG+20%TOKAMAX SiC Whiskers	HP160 (1800°C) A-16SG+20%ARCO SiC Whiskers	HP171 (1800°C) A-16SG+20%ARCO SiC Whiskers
Density (g/cm^3)	3.76	3.80	3.78
Porosity (%)	.72	.26	.43
H_2O Abs. (%)	.19	.07	.11
% of theor. -density	98.3	99.3	98.8
Strength (Kpsi) (MOR Bars)	58.79	67.39	51.25
M.O.E. (Mpsi)	56.74	57.11	57.09

* The data in this table came from Alcoa.

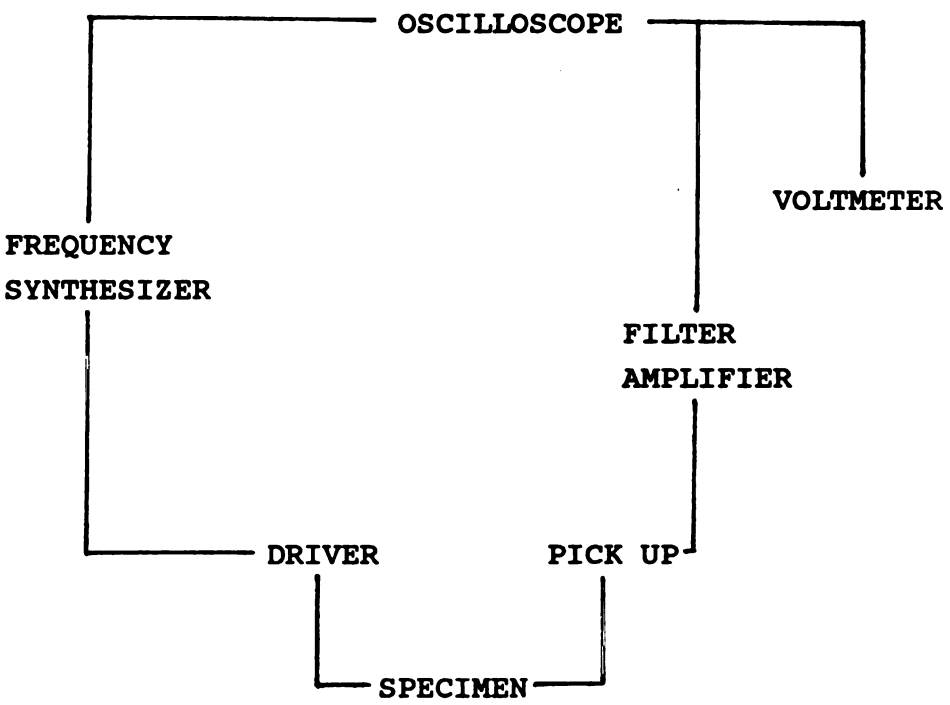

Figure 5. Outline of apparatus for measuring the elastic modulus (Dynamic resonance method).

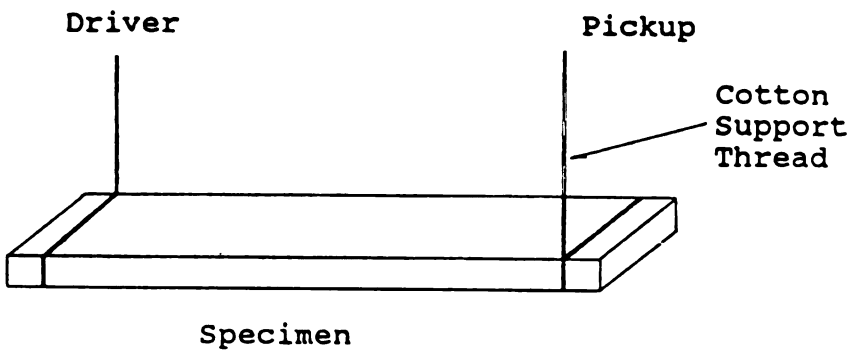

Figure 6. Illustration of method of coupling accoustic energy.

was amplified and converted into mechanical vibrations via a high power piezoelectric driver transducer (model number 62-1 made by Astatic Corp., Conneaut, Ohio). And it was allowed to pass through the specimen, and converted from a mechanical to an electronic signal by the pick up transducer. This signal was amplified, filtered (4302 Dual 24DB/Octave Filter-Amplifier made by Ithaco, Ithaca, N.Y.), and passed through a voltmeter (8050A Digital Multimeter made by Fluke, Everett, WA), and oscilloscope (V-100A 100MHz Oscilloscope made by Hitachi, Japan).

Resonance frequencies for the polymer composites were found to be the sharp. The maximum amplitude of the vibration and the mode of vibration were determined by probing the specimen with a needle to determine nodal plane locations. To calculate the elasticity, one must know the type and the mode of the vibration of the specimen. A prismatic bar can be excited in a variaty of vibrational modes, including the fundamental flexural frequencies. Thus if one identifies a resonant frequency, one must determine which particular mechanical vibrational mode is being excited before a determination of elastic modulus can be made. The vibrational mode can be identified by locating the position of the vibrational nodes and antinodes along the specimen in which a standing-wave vibration forms. The positions of the nodal and antinodal lines on a prismatic bar-shaped specimen vibrating at a mechanical resonance may be determined by

mechanically probing the bar [17].

In this study, the nodal and antinodal positions were probed using a sewing needle, balanced at various locations along the length of the resonating bar. When the needle is on a nodal line, the amplitude of resonant frequency will change very little. But if the needle is positioned away from a nodal line, then the needle will dampen the mechanical vibrations in the specimen, and the vibrational amplitude, as measured by the pick-up transducer, will be reduced. Anderson [17] indicates the position of the nodes as a fraction of the length of the specimen (Table 5).

The resonant frequency was taken as the average of five or more readings. This experiment was done at room temperature.

The resonance frequency data were converted into moduli values by using the equations of Pickett [18] as modified by Hasselman [19]. They were computer programmed by E. D. Case. Shear modulus, G, was calculated from the equation

$$G = P\,(2L*f/N)^{2}\,*R \qquad (5)$$

where N = an integer (unity for the fundamental mode)
f = torsional resonance frequency
L = specimen length
P = mass density
R = a shape factor.

Table 5. Position of the Vibrational Modes of a Prismatic Specimen. The Nodal Positions are Expressed as Function of the Length of the Specimen.

Mode of Vibration	Flexural Vibration	Torsional Vibration
Fundamental	0.224	0.500
	0.776	
First Overtone	0.132	0.250
	0.500	0.750
	0.868	

For prismatic specimens of rectangular cross section, R can be approximated by an equation as follows;

$$R = \{[1+(b/a)^2]*[1+(0.0085N^2b^2/L^2)] / [4-2.521 (a/b)[(1-1.991)/(\exp(b/a)+1)]]\} - 0.06(Nb/L)^{1.5}(b/a-1)^2 \quad (6)$$

where a = thickness of specimen
b = width of specimen.

Young's modulus, E, for a rectangular specimen can be obtained from the equation

$$E = 0.94642PTf^2L^4/D^2 \quad (7)$$

where f = fundamental flexural resonant frequency
L = length of the specimen
P = mass density of the material
T = a shape factor
D = cross sectional dimension in the direction of vibration.

The shape factor T is approximated by

$$T = 1 + 6.58(1+0.0752\nu +0.8109\nu^2)(D/L) - 0.868 (D/L)^4 - [8.34(1+0.2023\nu+2.173\nu^2)(D/L)^4] / [1+6.338(1+0.148\nu+1.53\nu^2)(D/L)] \quad (8)$$

where ν = Poisson's ratio.

3-3. Room Temperature Internal Friction Measurement

Internal friction (Q^{-1}) may be determined in two ways using Forster's method [16].

For the polymer composite having a high damping property, the full width half maxima method is most effective and accurate. For the full width half maxima method, the same equipment was used as employed for measuring elastic modulus. The peak width, Δf, can be measured by finding the two values of frequencies at which the amplitude of vibration is one-half the value of resonance. The measured internal friction, Q_m^{-1}, is given by

$$Q_m^{-1} = 0.5773 * \Delta f / f \qquad (4)$$

where f = the resonance frequency.

The free decay method is more effective with the specimen having smaller values of internal friction such as the SiC/Alumina composite. For the free decay method, two additional items of apparatus (trigger* and counter**) are required. Figure 7 shows the "internal friction apparatus" for the free decay method. With the specimen

---

* Constructed by the Biochemistry Electronics Shop, Michigan State University

** Model 5314A Universal Counter made by Hewlett-Packard

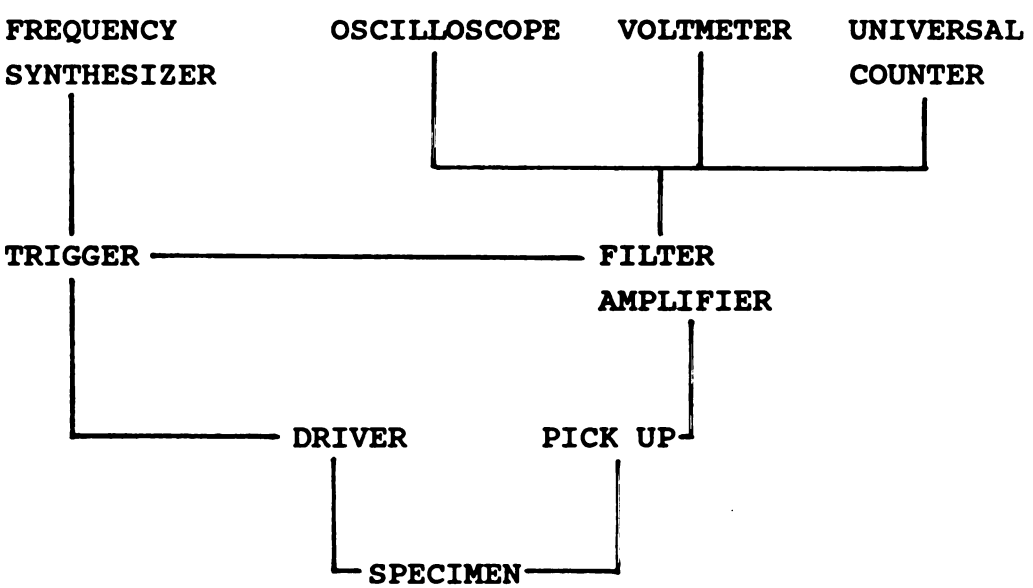

Figure 7. Internal friction apparatus diagram.

driven at its fundamental flexural resonant frequency, the driving signal is turned off by changing the mode from drive to free decay and the number of cycles, N, between a fixed amplitude, A, and a smaller fixed amplitude, B, is counted. The measured internal friction, Q_m^{-1}, is given by

$$Q_m^{-1} = \ln(A/B)/\pi N. \qquad (5)$$

The measured internal friction, Q_m^{-1}, is composed of the internal friction of the specimen, Q_s^{-1}, and the internal friction of the apparatus, Q_a^{-1}. The internal friction of the apparatus includes the effects of the specimen suspension position.

Wachtman and Tefft [14] have formulated an equation relating Q_a^{-1} and Q_s^{-1} to the measured internal friction, Q_m^{-1},

$$Q_m^{-1} = [Q_s^{-1} + kQ_a^{-1}(Y/Y')^2]/[1+k(Y/Y')^2] \qquad (10)$$

where Q_s^{-1} = the internal friction of the specimen
k_1 = an empirical constant
Q_a = the internal friction of the apparatus
Y = the vertical displacement of the suspension point from equilibrium
Y′ = the vertical displacement of the end of the specimen.

The Y/Y′ term is given by Rayleigh [20] for the transverse fundamental mode of vibration as

$$Y/Y' = [1.018(\cosh 4.730x/l + \cos 4.730x/l) - (\sinh 4.730x/l + \sin 4.730x/l)]/2.036 \quad (11)$$

where l = the length of the specimen
x = the distance to the suspension point from the end of the specimen.

These equations were also computer programmed by E. D. Case.

More than three pairs of suspension positions were marked on each specimen (Figure 6 illustrates the suspension of the specimen). The horizontal distance, x, from the end of the specimen was measured using metric vernier calipers. The specimen was suspended by cotton string and internal friction was measured for the each pair of suspension positions. The measured Q_m^{-1} were put into the program to obtain values for Q_a^{-1}, k and Q_s^{-1}. The average of three successive determinations of the internal friction of the specimen was taken as the value of the internal friction of the specimen. All of these determinations of Q_s^{-1} were made in air, neglecting the damping effect of air.

3-4. Elevated Temperature Elastic Moduli and Internal Friction

In addition to the full width half maxima method and the free decay method described in the section 3-3, there are other methods of measuring internal friction at room temperature. For example, the quartz crystal composite-oscillator method (ultrasonic pulse method) is capable of giving very accurate measurements of small values of internal friction. However, Forster's method is capable of being extended to elevated temperature by the simple adjustment of surrounding the specimen with a furnace, as shown in Figure 8.

Elevated temperature data were obtained by suspending the specimen horizontally by platinum wire (Ted Pella, Inc., Tustin, CA) in the hot zone of a electric resistance furnace. The heated chamber of the vertical furnace was 14 inches long and 4 inches in diameter. The temperature was controlled by a digital temperature controller (CN5000 Omega, Engineering Inc., Stamford, CT). The fundamental flexural resonance frequency was determined over the range from room temperature to 900°C, with the temperature being raised by 50°C increments.

The resonance frequency f_t at some temperature ΔT above room temperature was converted to relative elastic modulus E_t/E_0 using the relationship [17]

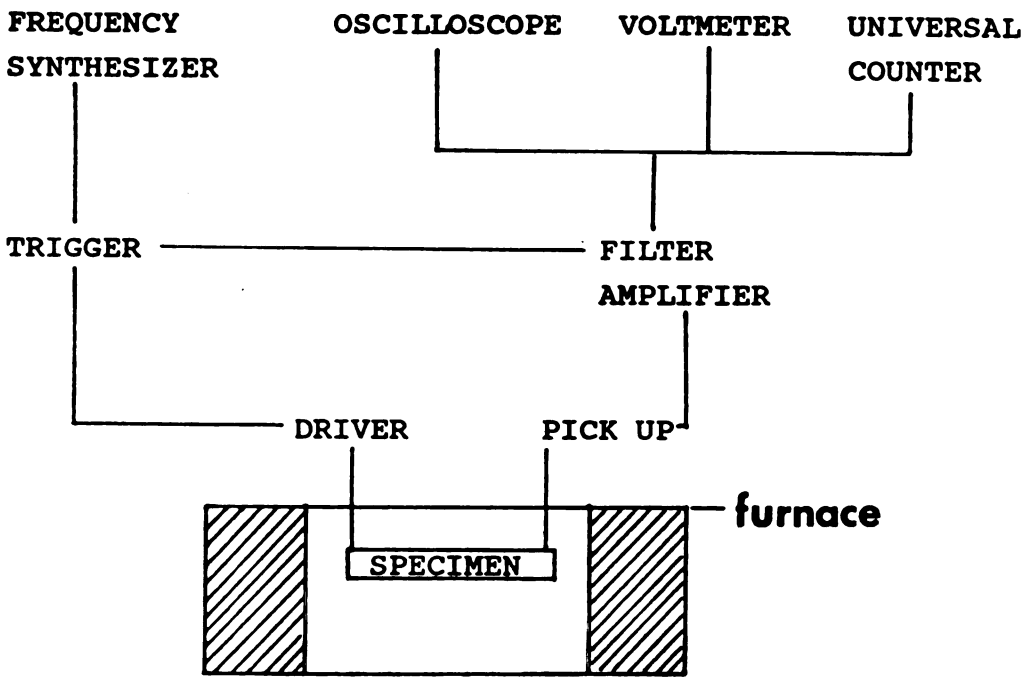

Figure 8. Schematic diagram of the elevated temperature elasticity and internal friction measurement apparatus.

$$E_t/E_0 = (f_t^2/f_0^2)/(1+\alpha\ \Delta T) \qquad (12)$$

where E_t, E_0 = high temperature and room temperature elastic modulus
f_0 = room temperature resonance frequency
α = linear thermal expansion coefficient.

The true internal friction value of the specimen was not measured at elevated temperature. Only one suspension point was used for elevated temperature internal friction measurements. Thus, these values were corrected to the specimen room temperature corrected internal friction value, Qs^{-1}, by the equation (8)

$$Qst^{-1} = Qs^{-1} (Qmt^{-1} / Qo^{-1}) \qquad (13)$$

where Qst^{-1} = the measured specimen corrected internal friction at elevated temperature
Qmt^{-1} = the measured internal friction at elevated temperature
Qo^{-1} = the measured internal friction with platinum wires in air at room temperature.

The assumption inherent in this equation is that the observed changes in internal friction as a function of temperature are due to changes in the internal friction of the specimen.

3-5. Dynamic Mechanical Tests

The dynamic mechanical properties of the polymer specimen were tested in a Du Pont 982 Dynamic Mechanical Analyzer. The specimen were heated at a rate of 5 °C/min to 75 °C in air. The tan delta, determined in this instrument as the ratio between the flexural loss modulus and the flexural storage modulus, and the flexural storage modulus were measured as a function of frequency.

3-6. Thermal Shock Fatigue Tests

For the SiC whisker reinforced alumina composite specimens, thermal shock fatigue tests were performed using the apparatus shown in Figure 9. The apparatus was designed to perform one thermal shock per hour. During one thermal shock, the specimen was suspended in the middle of the furnace for approximately 45 minutes. After thermal shock, the specimen remained in the water bath for 15 minutes.

The furnace used in this study was an electric resistance furnace. The heated chamber of the furnace was 13.5 inches long and 3 inches in diameter. The power input to the furnace was controlled by a variable transformer (2PF136 type Powerstat, The Superior Electric Co., Bristol, Conn). The variable transformer was adjusted to a predetermined power level and the furnace

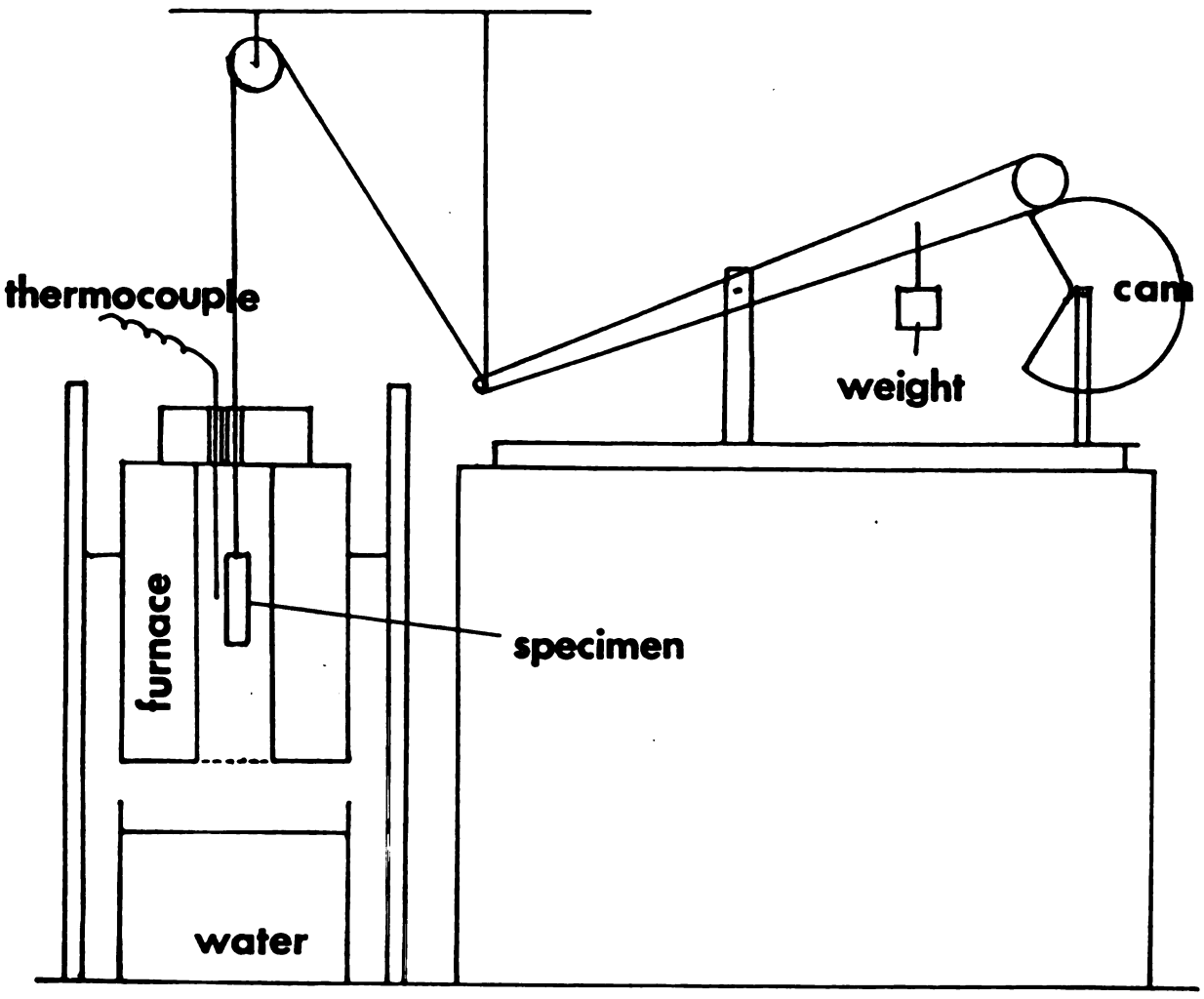

Figure 9. Schematic diagram of the thermal shock test apparatus.

was allowed to approach thermal equilibrium before operating the thermal fatigue equipment. Up to two and one-half hours was required for thermal equilibrium to be reached. Once thermal equilibrium was reached, the change in thermocouple output was ± 1 millivolt during the entire thermal shock anneal, which is equivalent to ± 2 degrees Celcius uncertainty. Temperature measurement was made with a J type thermocouple with its hot junction located to the side of the sample near its middle.

The plastic container for the water bath was rectangular with dimensions 24cm x 50cm x 75cm. Approximately 8 liters of distilled water were used for the water bath. The temperature of the water bath was measured by a mercury-in-glass thermometer with a temperature range of -10 degrees Celsius to 260 degrees Celcius. The thermometer markings were at 1 degree Celcius intervals, so temperature measurements were accurate to within ± 0.1 degree Celcius.

After attaining the preselected temperature in the middle of the furnace, the thermal shock fatige tests were performed. Rapid thermal quenching was done one time per hour. The typical time interval for the specimen free fall between the furnace and the water bath was one second. An electric timer was used to measure the dropping time. All specimens were removed from the water bath after having the desired number of thermal shocks. Specimens were dried with a paper towel and kept 10 hours

at room temperature before performing the elasticity and internal friction measurements.

The thermal shock damage was examined by measuring the changes in the elastic modulus and internal friction.

4. RESULTS AND DISCUSSION

4-1. Polymer Composite

Values of the resonant frequency, Young's modulus, shear modulus and internal friction at room temperature are given in Table 6 for the unidirectional fiber composites included in this study. In Table 7, DMA (Dynamic Mechanical Analyzer) results are listed.

Unidirectional composites are anisotropic due to their nature, thus their properties show a marked differences as a function of direction. The polymer composites in this study are unidirectional, hence a modulus anisotropy and a internal friction anisotropy are expected. The Young's modulus anisotropy, E(longitudinal)/E(transverse), varied from a value of 11.6 to 12.4. The internal friction anisotropy, Q^{-1}(transverse)/Q^{-1}(longitudinal), varied from a value of 7.5 to 8.6.

Although for the present study, internal friction was always higher in the transverse direction, the Young's modulus was always higher in the longitudinal direction. Ledbetter [22] observed similar directional dependences for the elastic moduli and internal friction of fiber reinforced polymer composites. According to Ledbetter [22], longitudinal specimens showed higher Young's modulus

Table 6. Modulus and Internal Friction of Polymer Composite

	Flexural Frequency (Hz)	Torsional Frequency (Hz)	E (Gpa)	G (Gpa)	Q^{-1} (10^{-4})
AU4 (longitudinal)	2627.5	1927.5	96.73	4.33	30.7
(transverse)	1039.5	2037.5	7.81	4.11	235.8
AS4 (longitudinal)	3468.6	2231.3	90.32	4.11	27.7
(transverse)	1074.3	2285.4	7.42	3.70	237.7
AS4C(longitudinal)	5115.0	2292.0	82.46	3.70	25.5
(transverse)	847.9	2215.6	7.09	3.67	190.9

Table 7. DMA Data for Polymer Composite at 35 Degrees Celcius (Modulus and Tan δ)

	0.1Hz	1.0Hz	10Hz	resonance
AS4 (longitudinal)				(42.9Hz)
E (Gpa)	42.75	43.15	44.32	49.30
Tan δ	0.00018	---*	0.00129	0.00642
(transverse)				(14.76Hz)
E (Gpa)	5.43	5.43	5.46	5.50
Tan δ	0.01500	0.00704	0.00858	0.00363
AU4 (longitudinal)				(41.95Hz)
E	43.16	43.57	44.76	53.35
Tan δ	0.00173	0.00121	0.00642	0.00634
(transverse)				(14.75Hz)
E	5.79	5.86	5.90	6.05
Tan δ	0.01124	0.00959	0.00840	0.00592

* DMA didn't read data at this point.

and lower internal friction than comparable specimens with transversely oriented fibers.

For the fiber reinforced composites included in the present study, the shear modulus was almost the same for two different directions (longitudinal and transverse fiber orientations). Figure 10 schematically illustrates the elastic moduli of the randomly mixed composite and a unidirectional composite as a function of fiber orientation [21].

Ledbetter [22] observed the dynamic Young's modulus and internal friction of several fibrous composites (including graphite-epoxy, glass cloth-epoxy, Boron-Aluminum and Boron-epoxy) at room temperature. The data obtained from the present study agrees well with the data obtained by Ledbetter. First, a higher Young's modulus corresponds to a lower internal friction, and vice versa. Second, Ledbetter's data also showed a modulus anisotropy, in that the modulus anisotropy varied from near 1 to 100, but in the present study a modulus anisotropy varied from 11.6 to 12.4. Ledbetter showed an internal friction anisotropy varied from 3 to 20. Ledbetter showed wide modulus anisotropy variation. However, the author didn't observe wide modulus anisotropy variation presumably because of the limited number of materials being measured.

An inverse relationship, between the longitudinal internal friction of the polymer composite and the interfacial shear strength, has been observed [23]. This

relationship is shown in figure 11. This suggests that the degree of the interfacial bonding can simply be characterized by using the measured value of internal friction of the polymer composite. Figure 11 shows that internal friction of a polymer composite (longitudinal) increases with decreasing the interfacial shear strength.

The measured room temperature internal friction, (Q_m^{-1}), as a function of specimen's suspension position is shown in figures 12-14. As predicted by Wachtman and Tefft [14], the measured internal friction varied with the position of the support strings. Figures 12-14 show that equation (10) fits the experimental data very well. For several polymer composite specimens, the measured internal friction values as a function of the specimen support position showed relatively good agreement with the theoretical internal friction values obtained by equation (10).

$$Q_m^{-1} = [Q_s^{-1} + kQ_a^{-1} (Y/Y')^2]/[1+k(Y/Y')^2] \qquad (10)$$

The internal friction values measured by sonic resonance method and DMA are different, even the author cannot find a trend between these two measurements due to the lack of data. The main reason for this difference may presumably come from the difference in the frequencies between these two method.

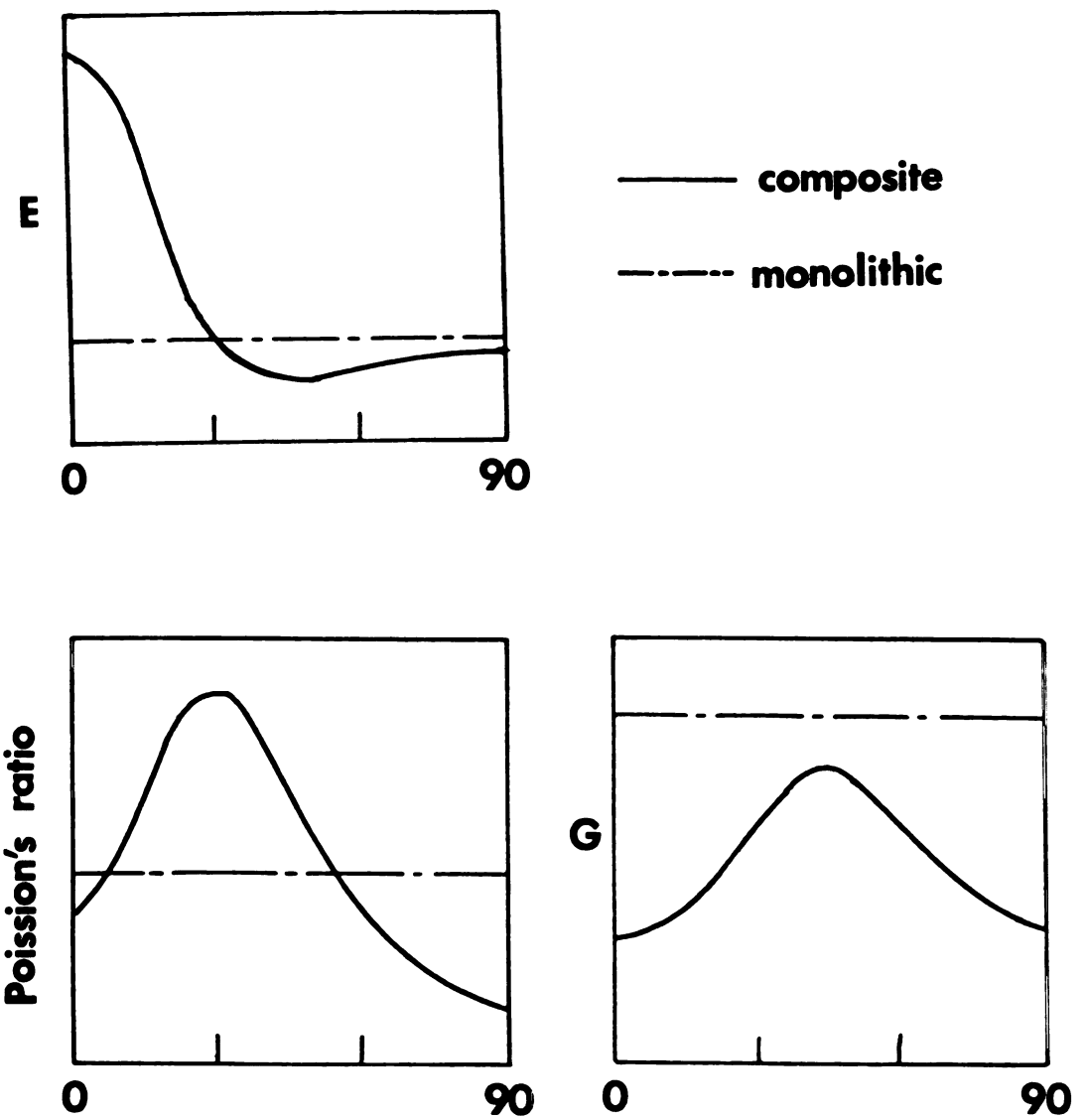

Figure 10. Variation of elastic moduli of a fiber composite and a monolithic material with the angle of reinforcement (After Meyer and Chawla [21]).

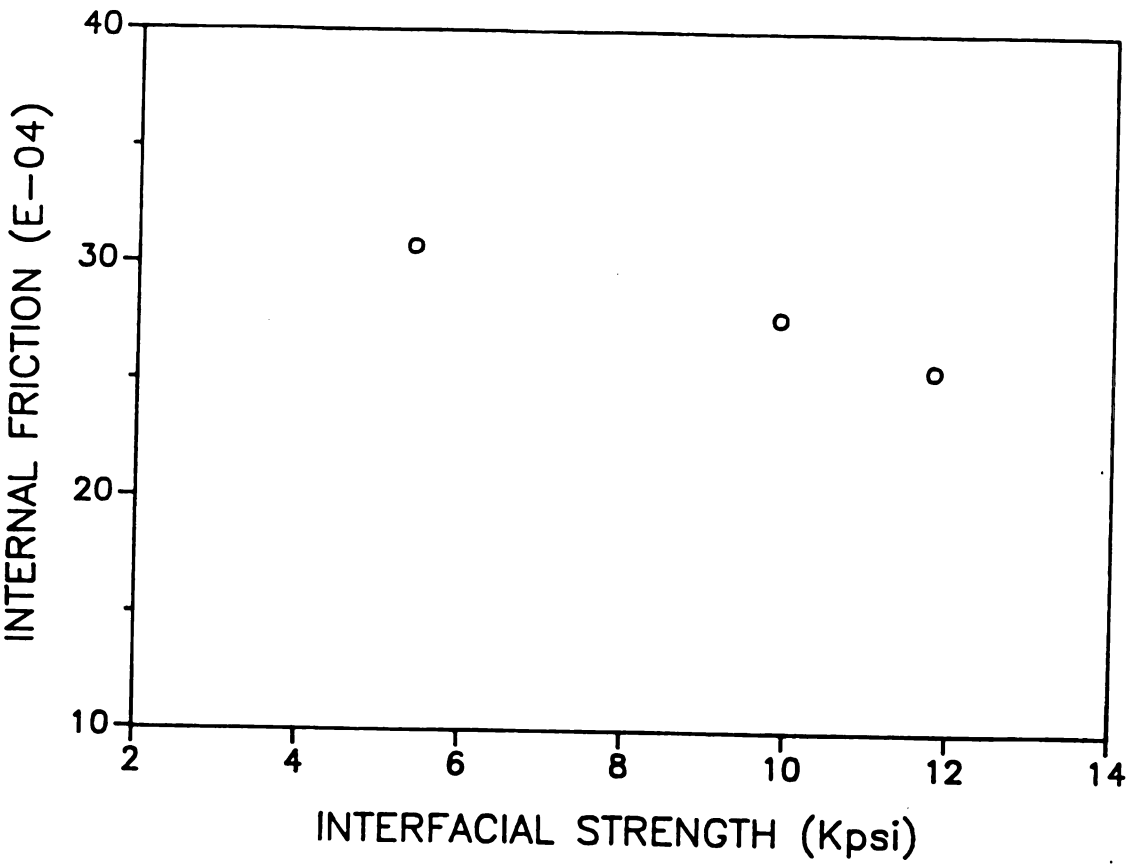

Figure 11. Internal friction of polymer composites as a function of interfacial shear strength.

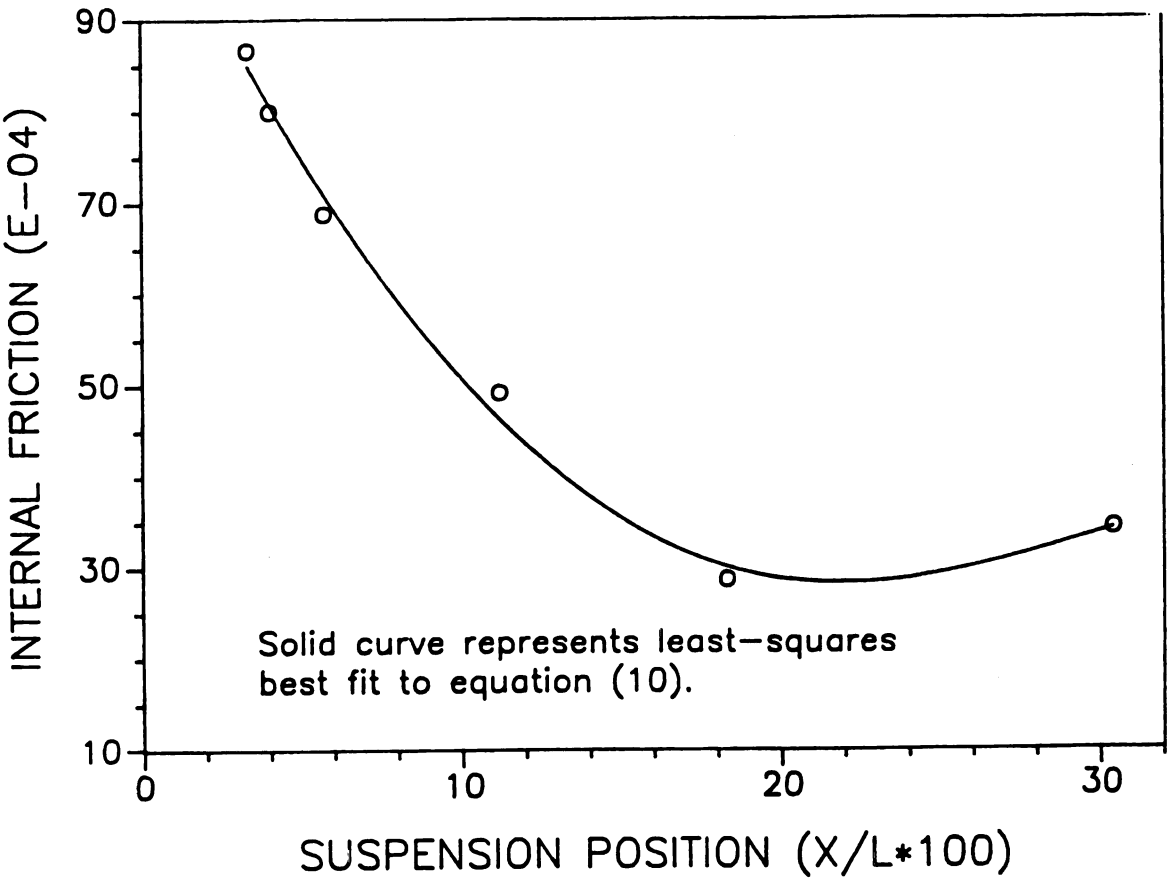

Figure 12. **Measured internal friction as a function of suspension position (x/l * 100) for the polymer composite specimen AS4-longitudinal.**

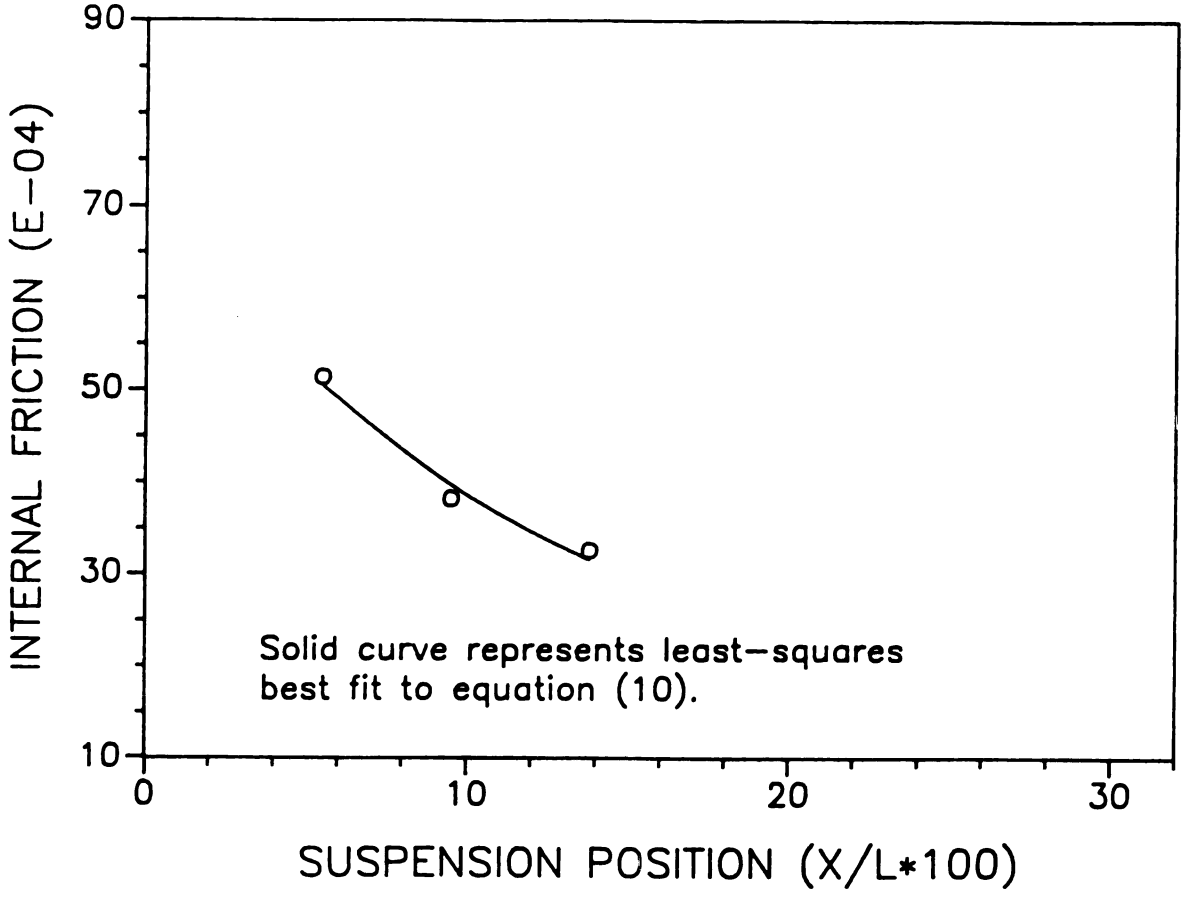

Figure 13. Measured internal friction as a function of suspension position (x/l * 100) for the polymer composite specimen AS4C-longitudinal.

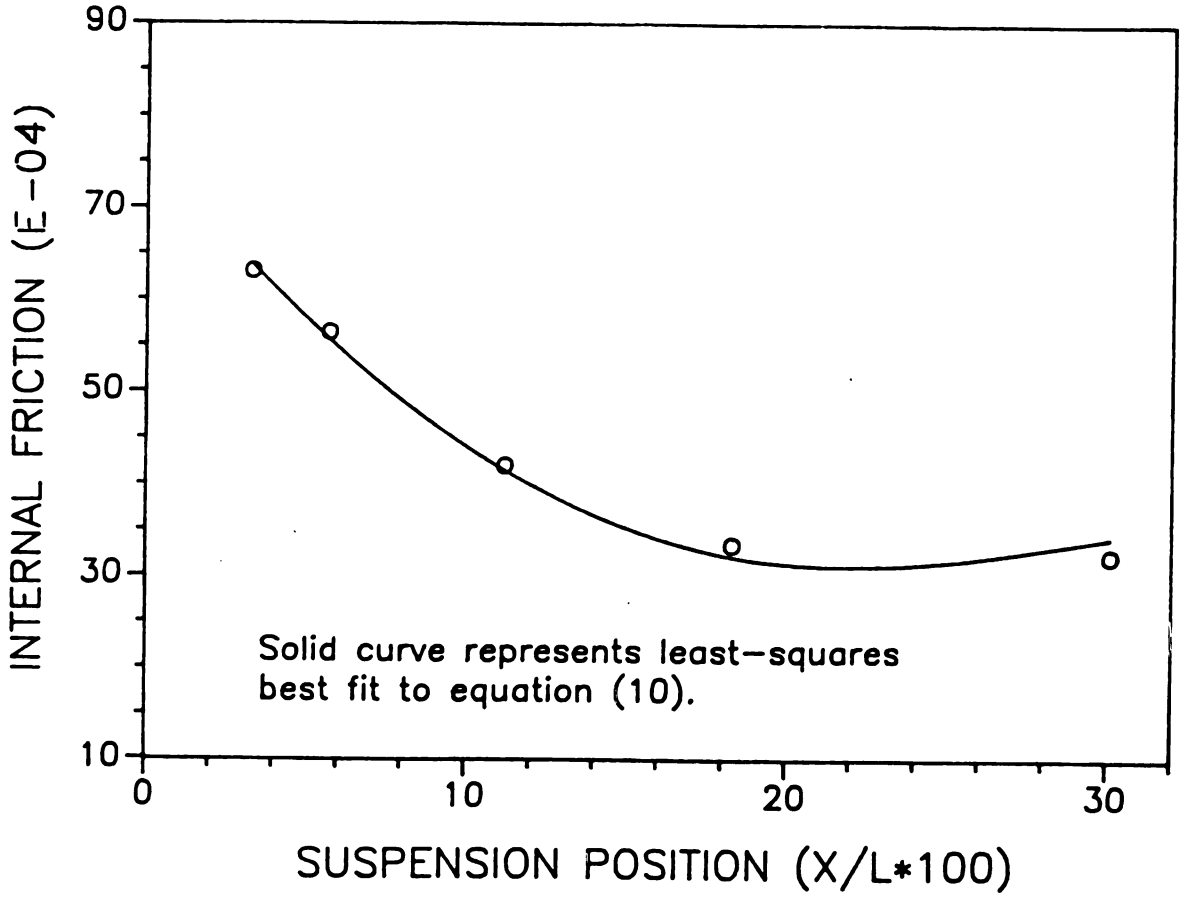

Figure 14. Measured internal friction as a function of suspension position (x/l *100) for the polymer composite AU4-longitudinal.

4-2. SiC Whisker Reinforced Alumina Composite

4-2-1. Room Temperature Modulus and Internal Friction

The room temperature resonant frequency, Young's modulus and internal friction of the as-received SiC whisker reinforced alumina composite specimens are given in table 8.

The Young's modulus values are 410.10 Gpa and 406.14 Gpa and the internal friction values 14.2×10^{-4} and 18.6×10^{-4} for the HP160 and HP171 specimens, respectively. Comparing the Young's modulus and internal friction observed for HP160 and HP171, it appears that the only difference between the two specimens is their porosity (density). The higher Young's modulus and lower internal friction value of HP160 may be attributed to the lower porosity (higher density). The strength data further supports this since the fracture strength decreases rapidly as porosity increases. Specimen HP158 cannot perhaps be compared directly because different whiskers were used in this specimen. Whiskers used for the specimen HP158 were TOKAMAX SiC whiskers, but for the specimens HP160 and HP171, ARCO SiC whiskers were used. However, it has not been demonstrated whether the mechanical properties of the TOKAMAX SiC whiskers and the ARCO SiC whiskers differ significantly. Thus, the use of fibers from different vendors may make no significant

Table 8. Room Temperature Modulus and Internal Friction of Alumina/SiC Composite Specimens

	Resonant Frequency (Hz)	E (Gpa)	Qs^{-1} (10^{-5})
HP158	6387.67	404.56	13.2
HP160	6406.17	410.10	14.2
HP171	6431.00	406.14	18.6

difference in the measured elastic moduli and internal friction. The values of mass density, porosity, water absorption, fracture strength, and elastic modulus (Table 4) measured by Alcoa were quite similar for each of the three SiC whisker/alumina matrix specimens. In this study, the room temperature values of elastic modulus and internal friction (prior to thermal shock, Table 8) were also quite similar for each of the three specimens.

Figures 15-17 illustrate the measured internal friction, Q^{-1}, as a function of the position of suspension, for the SiC whisker reinforced alumina composites.

4-2-2. Elevated Temperature Modulus and Internal Friction

Prior to thermal shock testing, the Young's modulus and internal friction were measured as a function of temperature for the as-received SiC whisker/alumina composite specimen HP171.

Figure 18 illustrates the Young's modulus as a function of temperature for SiC whisker/alumina composite HP171. The modulus decreased continuously with increasing temperature, which is typical of polycrystalline ceramics. Also, the modulus retraced the heating paths during cooling. The modulus changed linearly up to 900°C, which was the maximum test temperature for the present study.

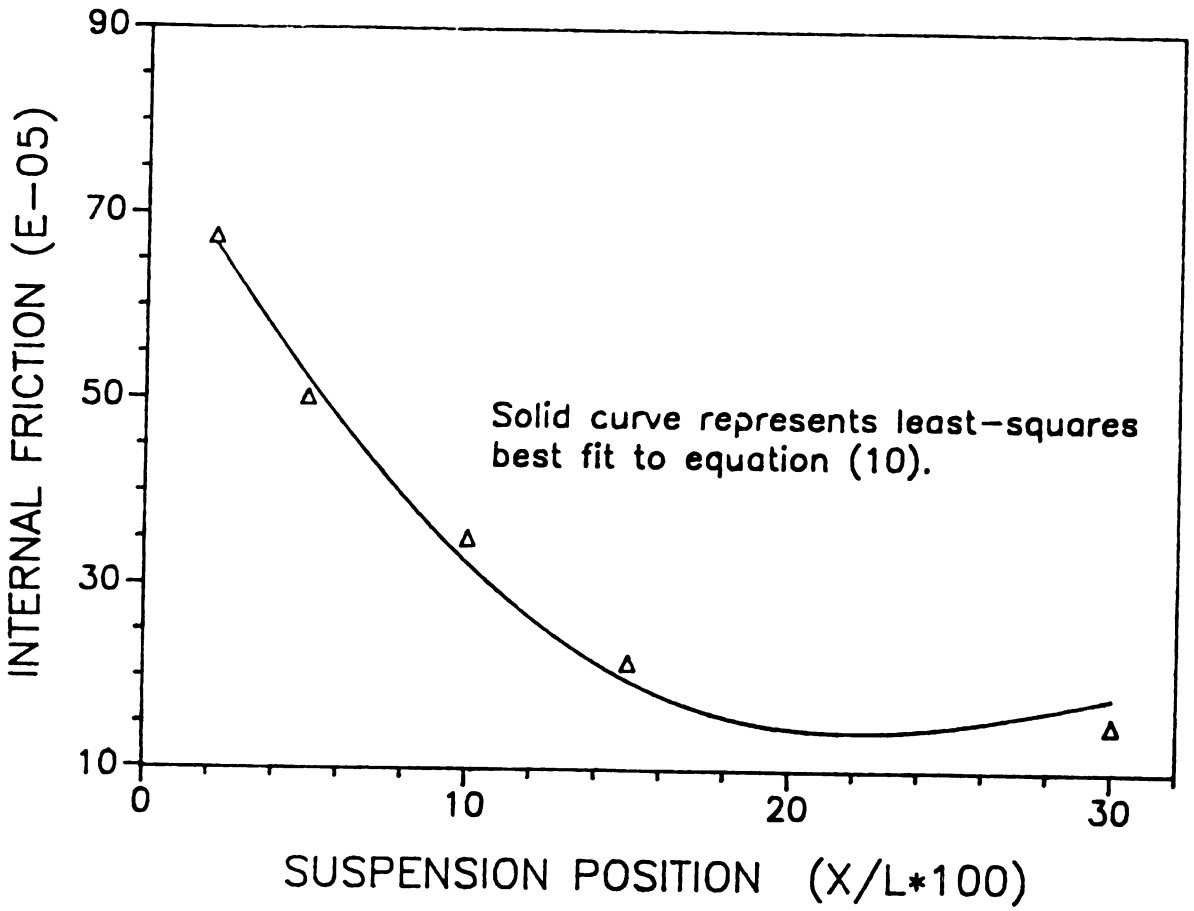

Figure 15. Measured internal friction as a function of suspension position (x/l *100) for the alumina/SiC composite specimen HP158.

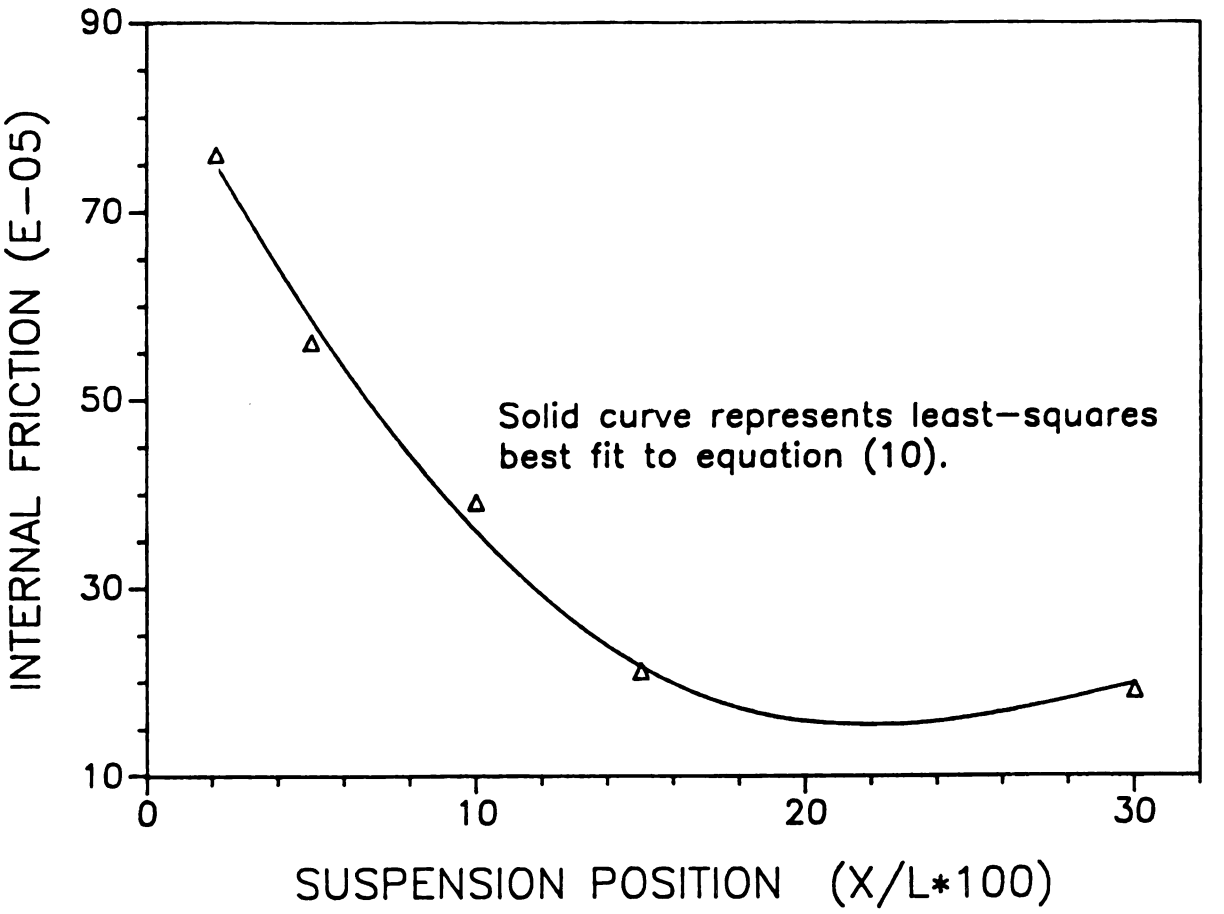

Figure 16. Measured internal friction as a function of suspension position (x/l *100) for the alumina/SiC composite specimen HP160.

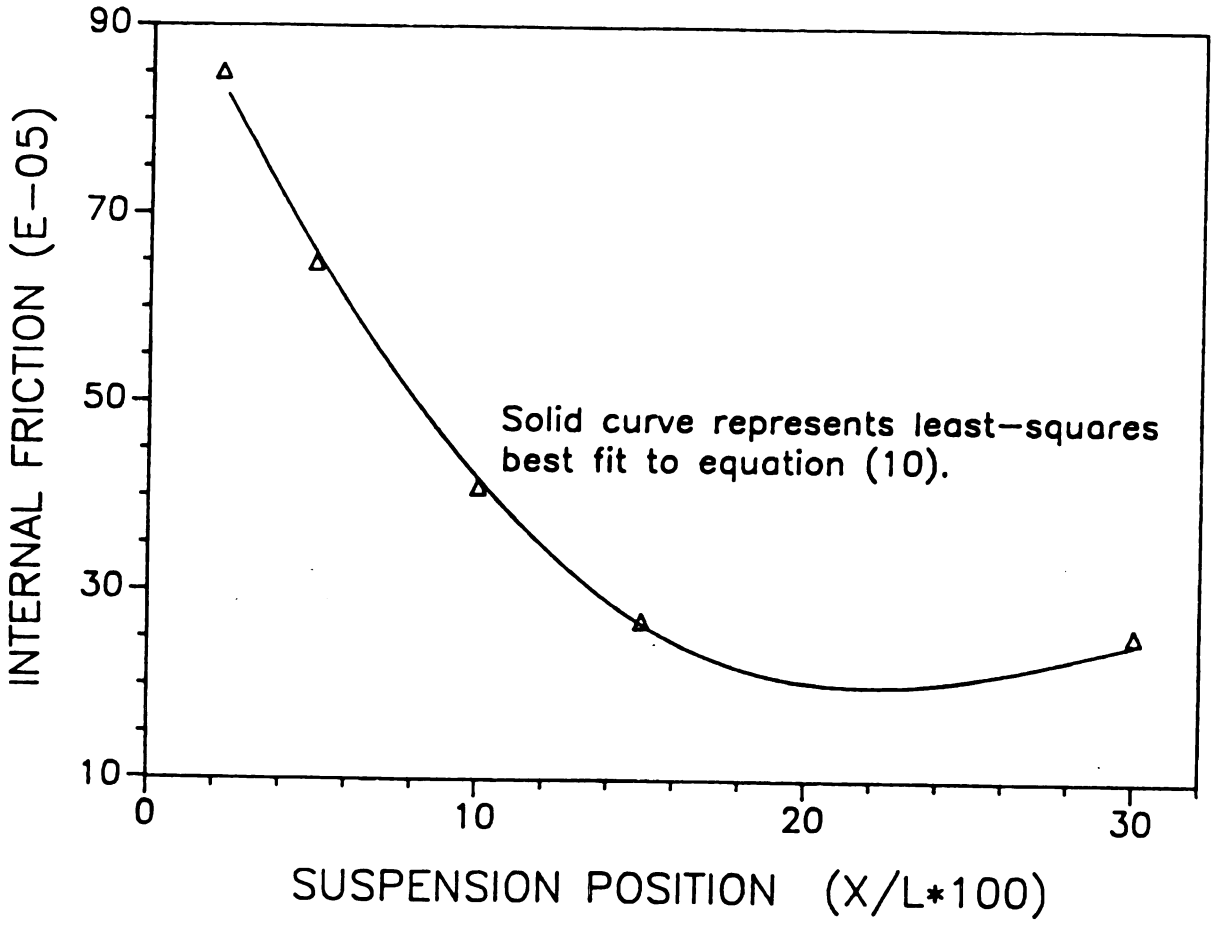

Figure 17. Measured internal friction as a function of suspension position (x/l *100) for the alumina/SiC composite specimen HP171.

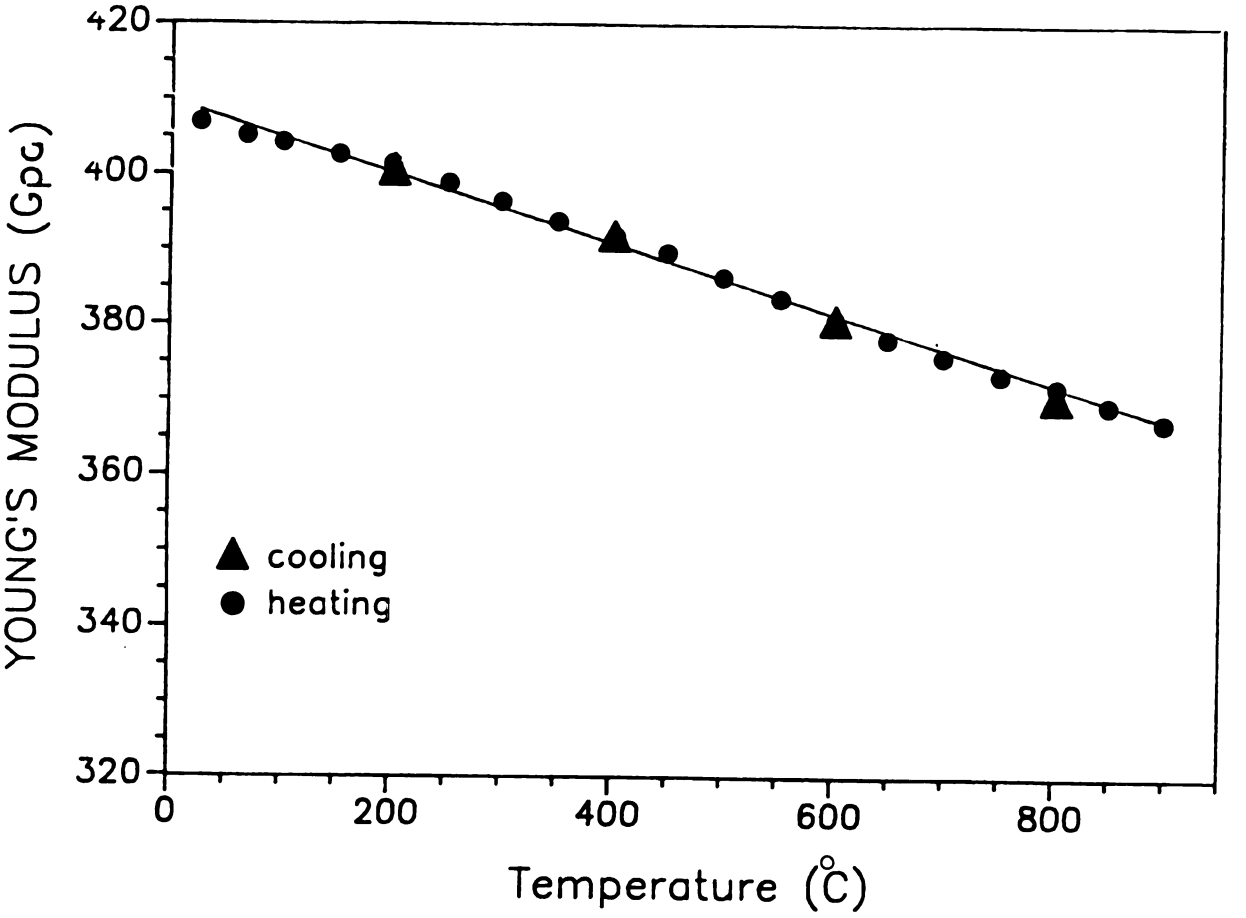

Figure 18. Young's modulus of the alumina/SiC composite specimen HP171 as a function of temperature (Measurements performed prior to thermal shock treatment of specimen HP171).

The modulus versus temperature data was fit via least-squares to a linear function of temperature. The least-squares procedure produced the empirical equation (in Gpa)

$$E = 409.5 - 0.047T \qquad (14)$$

The correlation coefficient for the least-square fit of the Young's modulus versus temperature data was 0.998 and the number of data points was 19. The linear relation indicates a modulus decrease of $\approx$ 1.1 percent/100°C which agrees favorably with data for various other polycrystalline ceramics [24,25]. In particular, the value of Young's modulus versus temperature slope for polycrystalline monolithic alumina has been determined to be 1.2 percent/100°C [26].

Figure 19 shows the internal friction, Q^{-1}, as a function of temperature, which was measured along with the modulus. The internal friction varied by approximately $\pm$ 30 percent about a mean value of 2.7×10^{-4}. The data do not yield a particulary smooth relation with temperature, but scatter of this type is typical for high temperature measurements of internal friction [8].

The room temperature internal friction value after this elevated temperature measurements has changed from 18.6×10^{-5} to 11.1×10^{-5}. The observed changes in internal friction during the measurements on unshocked specimen HP171 are relatively small compared to ΔQ_{max}, the maximum

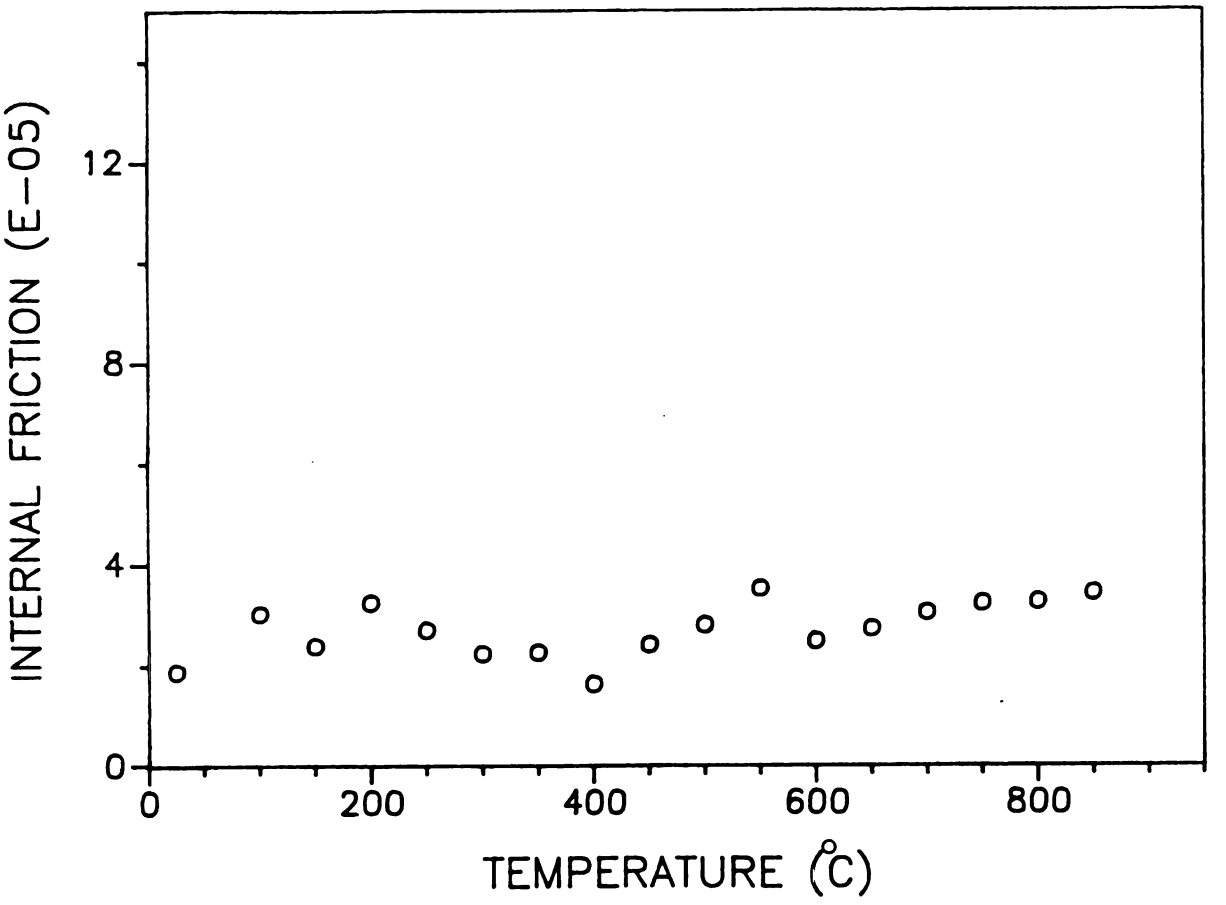

Figure 19. Internal friction of the alumina/SiC composite specimen HP171 as a function of temperature (Measurement performed prior to thermal shock treatment of specimen HP171).

change in internal friction due to the thermal fatigue testing that was performed as subsequent step of this study. Small changes in the internal friction could be due to relaxation of residual stresses in the specimen, or in part to diffusive crack healing (the anneal temperature of 900°C or equivalently 1173°K ≈ 1/2 melting temperature for the alumina matrix).

4-2-3. Thermal Fatigue Test

Figure 20 and figure 21 show the room temperature Young's modulus and internal friction of SiC whisker reinforced alumina plotted as a function of the number of thermal shock cycles. As expected, the internal friction increases while the Young's modulus decreases [5,6,7,9]. The changes in both Young's modulus and in internal friction are presumably due to the formation of microcracks that form due to the transient stresses the specimens experience during thermal shock.

This study shows that for thermal shocked SiC whisker reinforced alumina composite specimen HP160 the microcracking increases the internal friction by a factor of nearly 120 percent. However, the modulus values for this specimen differ only by a factor of 0.07 percent. A possible explanation is that specimen HP160 contains only a few microcracks and that internal friction measurements

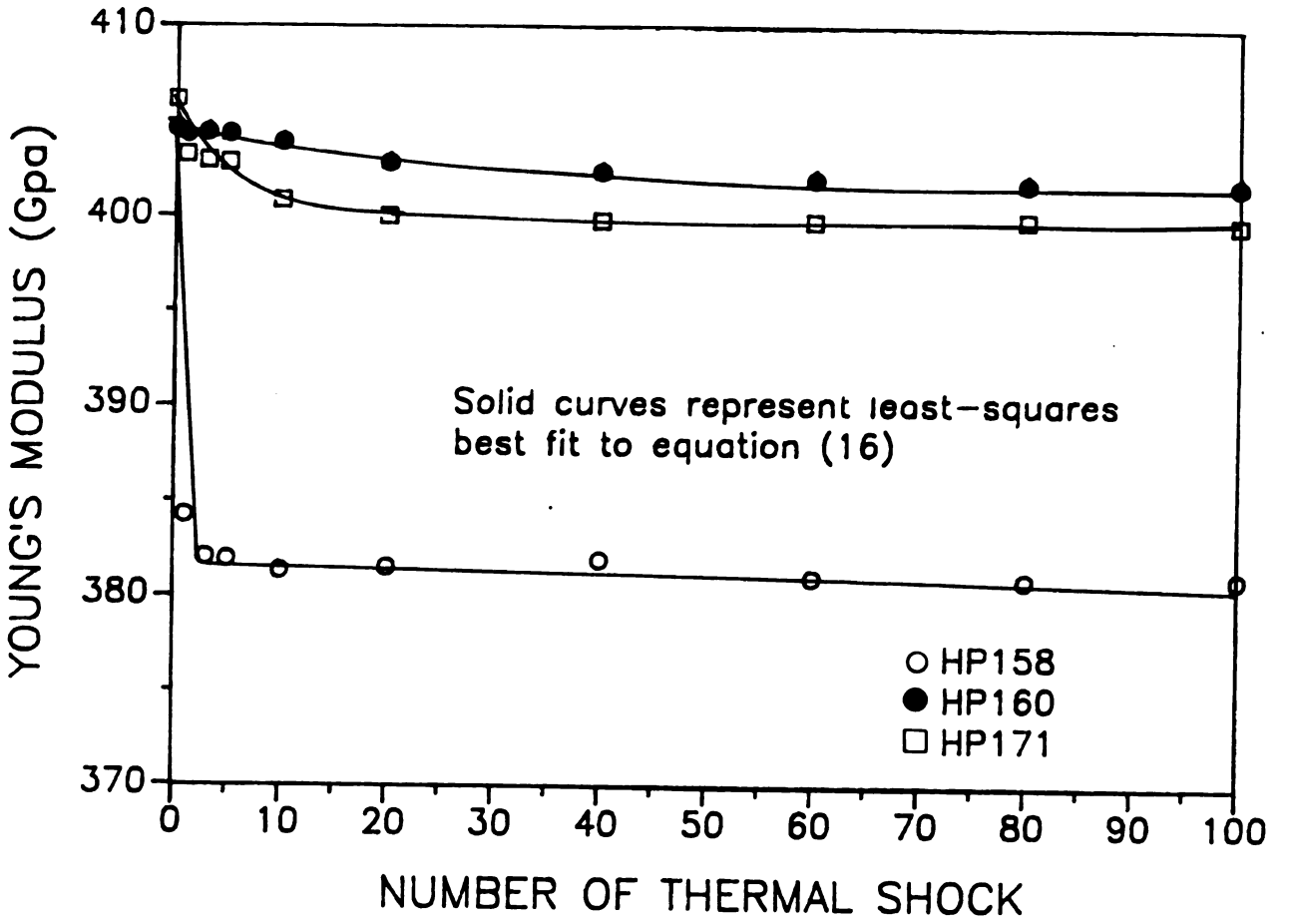

Figure 20a. Young's modulus of the alumina/SiC composite specimens HP160 (ΔT=270 degrees C), HP171 (ΔT=310 degrees C) and HP158 (ΔT=380 degrees C) as a function of thermal shock cycle.

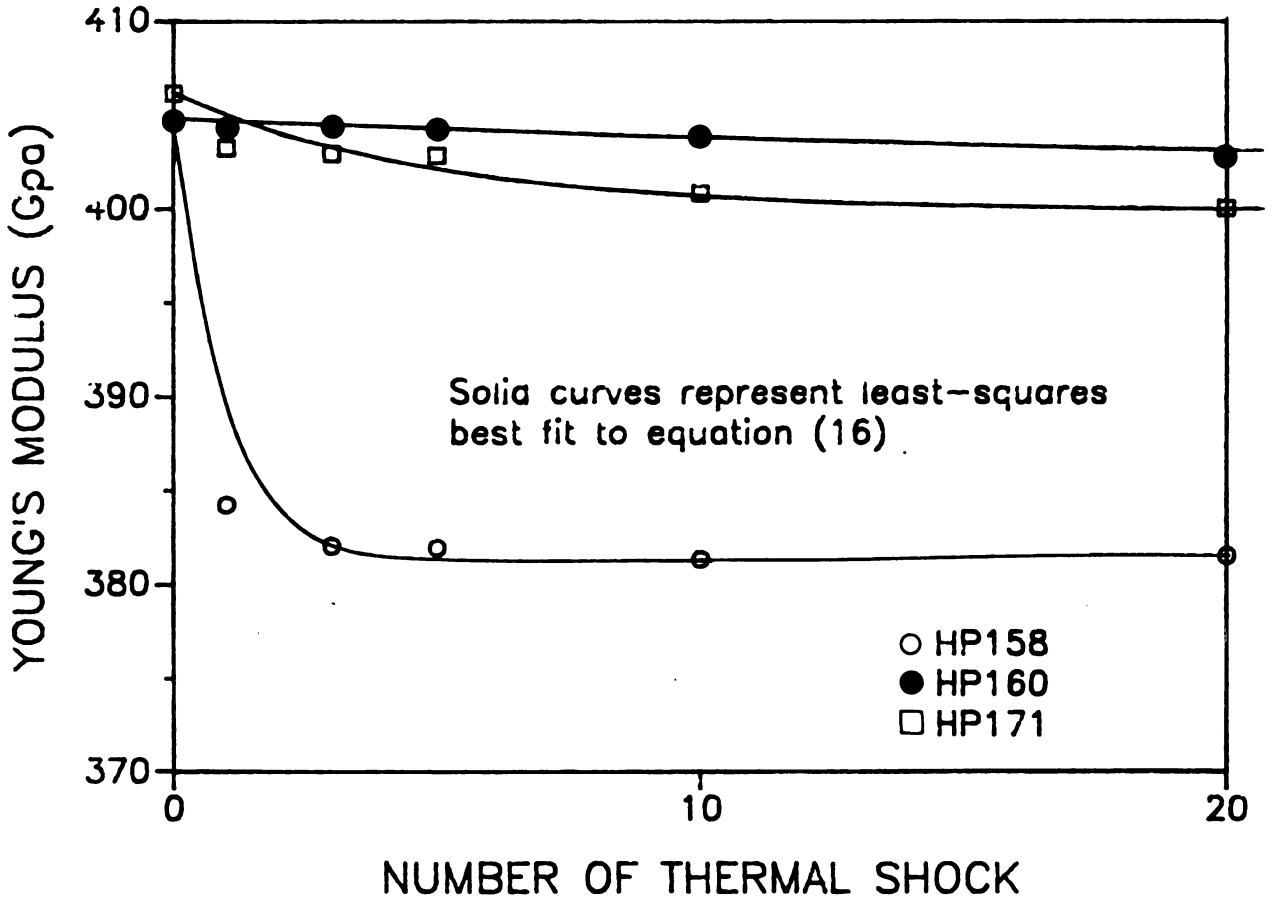

Figure 20b. Young's modulus of the alumina/SiC composites HP158, HP160, and HP171 versus thermal shock number. Data in this figure is a subset (namely, the first twenty thermal shocks) of the data presented in figure 20a. Note that even for n small, equation (16) fits the data well.

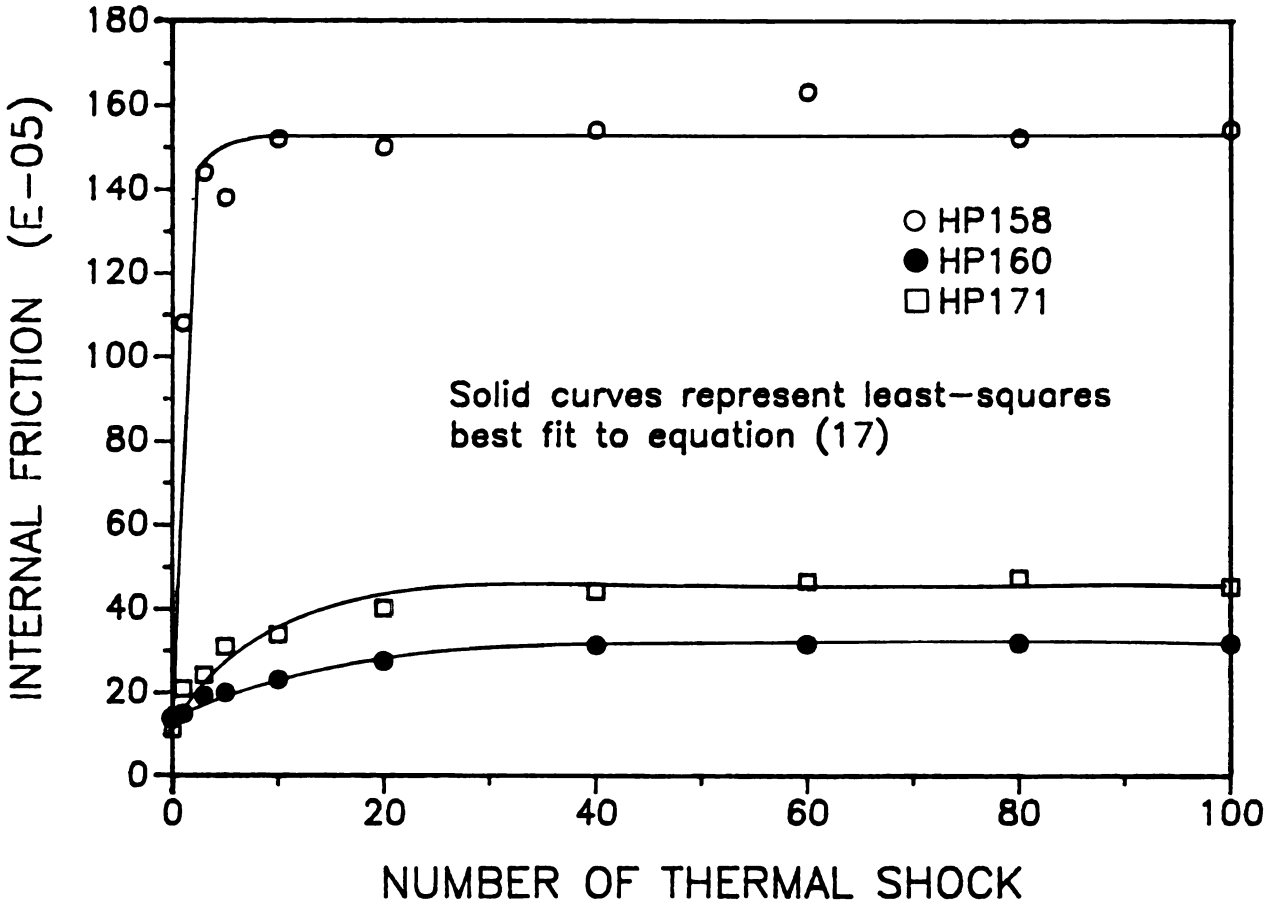

Figure 21a. Internal friction of the alumina/SiC composite specimens HP160 (ΔT=270 degrees C), HP171 (ΔT=310 degrees C) and HP158 (ΔT=380 degrees C) as a function of thermal shock cycle.

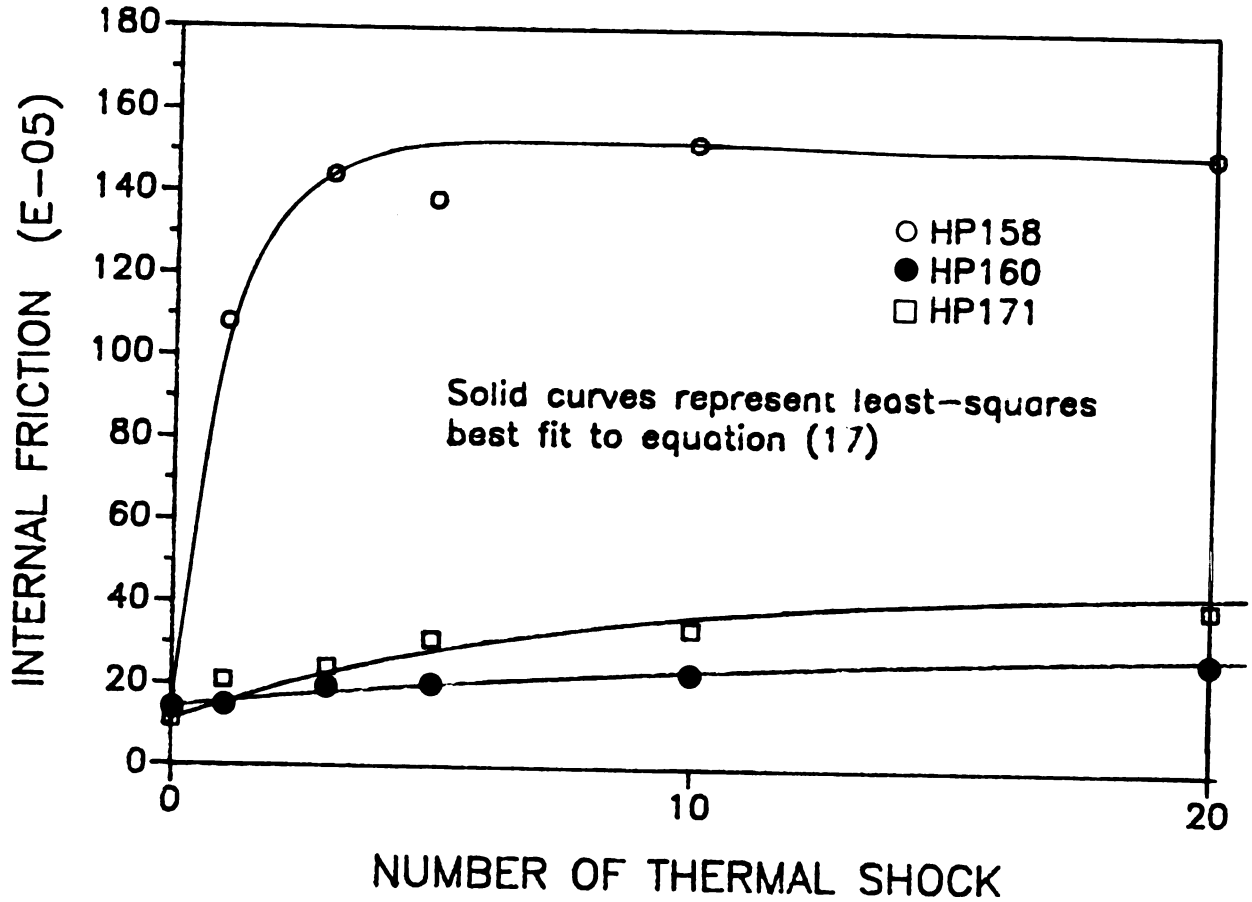

Figure 21b. Internal friction of the alumina/SiC composites HP158, HP160, and HP171 versus thermal shock number. Data in this figure is a subset (namely, the first twenty thermal shocks) of the data presented in figure 21a. Note that even for n small, equation (17) fits the data relatively well.

are more sensitive to the microcracking effects than are modulus measurements [7,27].

Relative changes in Young's modulus and internal friction are listed in table 9 for each of the three thermal shocked SiC whisker/alumina matrix composite.

The observed decrease in elastic modulus of the SiC whisker reinforced alumina specimens with increased thermal cycling can be explained quantitatively on the basis of microcrack damage acculmulation with increased thermal shock damage. The reduction in Young's modulus as a function of microcrack damage may be understood quantitatively from an equation of the form [28]

$$E = Eo\ (1-f(\nu)Na^3) \qquad (15)$$

where E = the effective Young's modulus
Eo = original Young'modulus
$f(\nu)$ = function of Poisson's ratio
ν = Poisson's ratio
N = microcrack density (number of microcracks per unit volume)
a = mean radius of microcrack.

The product, Na^3, is defined as the crack damage parameter, which shall be denoted here as ϵ. The effective modulus varies linearly with the crack damage parameter. The critical value of ϵ at which E vanishes is $1/f(\nu)$.

The data were fit to the empirical relations via non-linear regression analysis in the plotIT system. The

Table 9. Relative Changes in Young's Modulus and Internal Friction for the Thermal Shocked Specimen (SiC Whisker/Alumina Composites)

Specimen	ΔT ($^{\circ}C$)	$\Delta E_{max}/E_o * 100$	$\Delta Q^{-1}_{max}/Q^{-1}_o * 100$
HP160	270	0.07	120
HP171	310	1.72	318
HP158	380	5.83	1049

empirical equations of the forms are for Young's modulus, E

$$E = Eo - A(1-\exp(-\alpha n)) \qquad (16)$$

where E = the effective Young's modulus in Gpa
Eo = Young's modulus for theoretically dense, non-microcracked material
n = number of the thermal shock cycle
A,α = positive constants determined by the non-linear regression.

For internal friction, Q^{-1}, where the data was scaled by a constant factor of 10^{-5} to facilate the least-squares fitting procedure, the emprical equation employed was

$$Q^{-1} = Qo^{-1} + B(1-\exp(-\beta n)) \qquad (17)$$

where Q_{-1}^{-1} = the effective internal friction
Qo = internal friction for the non-microcracked material
B,β = positive constants determined by the non-linear regression.
n = number of the thermal shock cycle.

The results of the non-linear regression analysis are shown in table 10. For a fixed value of ΔT, the constant A in equation (16) represents a "damage saturation" or steady state level of damage for a large number of thermal shock cycles, n. Likewise, the constant B in equation (17) represents the large n value (or asymptotic value) of the internal friction. The thermal fatigue damage, as measured by both the internal friction and Young's modulus

Table 10. Results of the Non-linear Regression analysis for the SiC whisker/Alumina Composites

Specimen	HP160	HP171	HP158
ΔT ($^{\circ}C$)	270	310	380
Q_o^{-1} ($\times 10^{-5}$)	14.18	11.10	13.40
Eo (Gpa)	404.84	406.10	404.60
A (Gpa)	3.00	6.21	23.17
B ($\times 10^{-5}$)	20.38	33.65	138.31
α	0.042	0.220	2.11
β	0.061	0.150	1.11
cor. coeff. (A,α)	0.993	0.956	0.991
cor. coeff. (B,β)	0.996	0.978	0.991

shows a saturation level, and this saturation damage level increases with increasing ΔT.

The constant α in equation (16) is a "rate of decrement" of the Young's modulus as a function of thermal fatigue treatment. At a number of cycles given by $n = 1/\alpha$, the relative decrement in Young's modulus is $(1-e^{-1}) \approx 0.632$. In table 11, a fatigue constant n_{0_e} is listed, where $n_{0_e} = 1/\alpha$ for the given thermal shock conditions. Similarly, $n_{0_i} = 1/\beta$ is the fatigue constant for the thermal shock induced changes in internal friction. As shown in table 11, n_{0_e} decreases rapidly as ΔT increases, thus the number of thermal shock cycles required to reach the saturation damage level (which are approximately by $\approx 3\ n_{0_e}$ and $3\ n_{0_i}$ respectively) is a sensitive function of ΔT.

In order to understand the increase in the effective internal friction quantitatively, a quantitative relation between the effective internal friction and crack damage parameter, such as equation (15), is needed. From equation (15) and (16), one can express

$$Eo(1-f(\nu)\epsilon) = Eo - A(1-\exp(-\alpha n)) \qquad (18)$$

Solving equation (18) then yields

$$\epsilon = 1/f(\nu) * A/Eo * (1-\exp(-\alpha n)) \qquad (19)$$

Table 11. Thermal Fatigue Constants for the SiC Whisker Alumina Matrix Composite

Specimen	HP160	HP171	HP158
ΔT ($^{\circ}C$)	270	310	380
(A-Eo)/Eo	0.9924	0.9847	0.9427
$(B-Q_o^{-1})/Q_o^{-1}$	0.437	2.072	9.33
n_{oe}	24.3	4.83	0.50
n_{oi}	16.3	7.25	0.89

Multipling equation (19) by $f(\nu) * Eo/A$ and rearranging gives

$$\exp(-\alpha n) = 1 - Eo/A * f(\nu)\epsilon \qquad (20)$$

Taking the logarithm of each side of equation (20) and deviding by $-\alpha$ then yields

$$n = -1/\alpha * \ln[1-Eo/A*f(\nu)\epsilon] \qquad (21)$$

Substituting n from equation (21) into equation (17)

$$Q^{-1} = Qo^{-1} + B(1-(1-Eo/A * f(\nu)\epsilon)^{\beta/\alpha}) \qquad (22)$$

Salganik [29] developed an equation similar to the equation (15), which is

$$E = Eo\ (1-f(\nu_o)\epsilon) \qquad (23)$$

where $f(\nu_o) = 16(10-3*\nu_o)(1-\nu_o^2) / 45(2-\nu_o)$ (24)

ν_o = Poisson's ratio for the noncracked material.

The calculated value of Poisson's ratio, ν_o, was 0.22 (this study). The calculated value of $f(\nu_o)$ in equation (24) was 1.775. If we use Salganik's equation (23) instead of equation (15), then we can express internal

friction as a function of crack damage parameter only. The relation is as follows

$$Q^{-1} = Q_o^{-1} - B(1-(1-E_o/A * f(\nu_o)\epsilon)^{\beta/\alpha}) \qquad (25)$$

Equation (25) can be rewritten as follows

$$\Delta Q^{-1} = C^1[1-(1-C^2\epsilon)^{C^3}] \qquad (26)$$

The entire data set of internal friction as a function of theraml shock damage for the three SiC whisker/alumina matrix composite specimens were fit to the empirical relation given by equation (26) via non-linear regression analysis. The constants C^1, C^2, and C^3 were 13.55×10^{-5}, 250, and 1.143, respectively.

For sufficiently small $C^2\epsilon$, the term $(1-C^2\epsilon)^{C^3}$ in equation (26) can be written as $(1-C^2C^3\epsilon)$ using the binominal expansion theorem. Thus, equation (26) becomes

$$\Delta Q^{-1} \approx C^1C^2C^3\epsilon = D\epsilon \qquad (27)$$

The least-squares best fit of equation (27) gives a value of 4.17×10^{-2} for constant D. From the equation (26), the result of product $C^1C^2C^3$ was 3.87×10^{-2}. Therefore the equation (27) can be a relatively good approximation to the ΔQ^{-1} versus ϵ data for the thermally-shocked SiC whisker/alumina composites in this study. The correlation

coefficients for equation (26) and (27) were 0.998 and 0.997, respectively. Thus while both equations fit the data relatively well, equation (26) with three adjustable parameters of course fits the data better than equation (27), a simple linear equation with one adjustable parameter.

Figure 22 shows the internal friction change, ΔQ^{-1}, as a function of crack damage parameter, ϵ, for the SiC whisker/alumina matrix composites. As shown in figure 22, ΔQ^{-1} increases as ϵ increases.

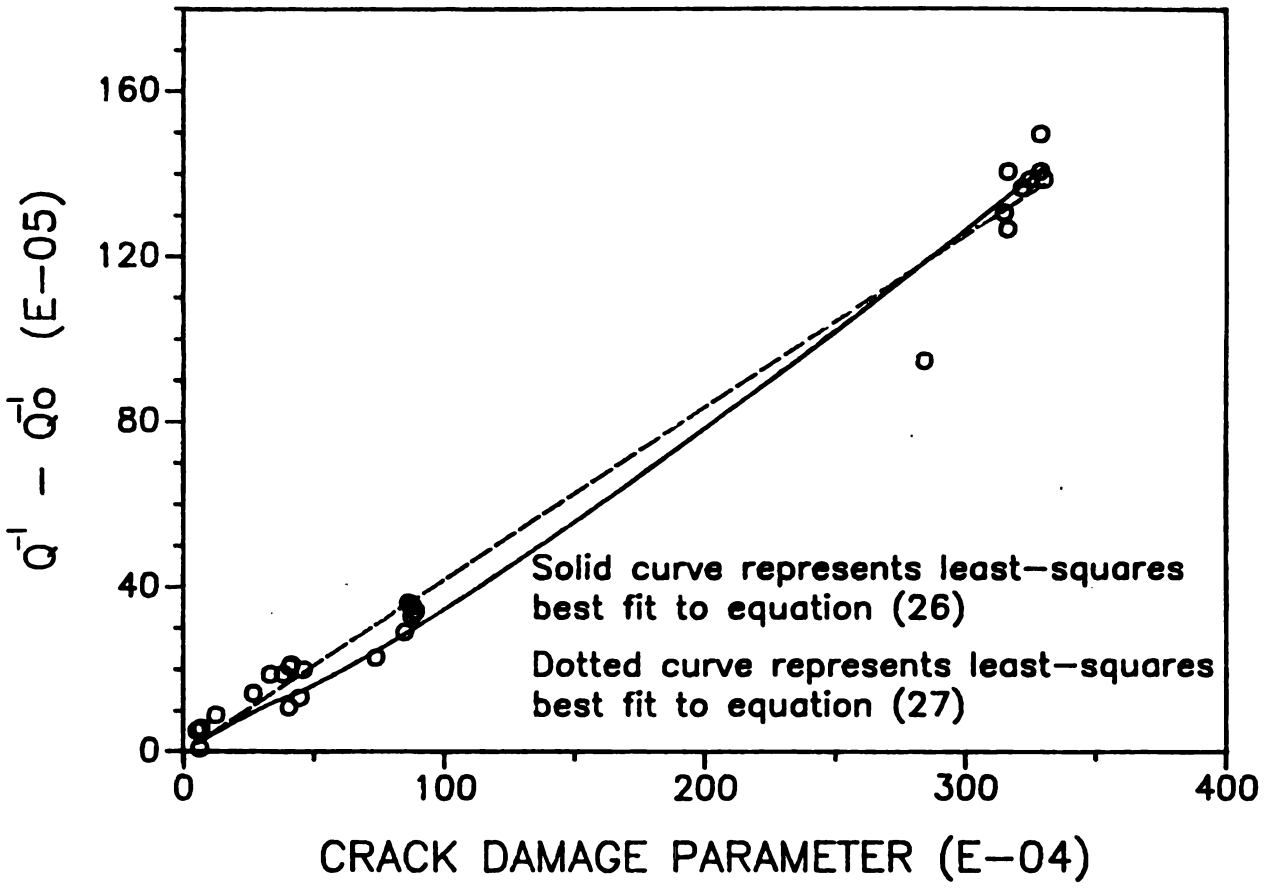

Figure 22. Internal friction change, ΔQ^{-1}, as a function of crack damage parameter, ϵ, for the SiC whisker/alumina composites.

CONCLUSIONS

This study dealt with both polymer and ceramic composites, although ceramic composites were the primary focus of the study.

Polymer composites reinforced with unidirectional fibers exhibited modulus and internal friction anisotropy. The internal friction increased with decreasing interfacial shear strength.

The elastic moduli of SiC whisker/Alumina decreased linearly with temperature at a rate of 1.1 percent/100 degrees Celcius. As thermal shock progressed, Young's modulus decreased and internal friction increased. Empirical equations for the modulus and internal friction as a function of thermal shock cycles were developed. The fitting equations were

$$E = Eo - A(1-(1-\exp(-\alpha n))$$

and $$Q^{-1} = Qo^{-1} + B(1-(1-\exp(-\beta n))$$

As ΔT increased, the "damage saturation" A, B, and the "rate of decrement or increment" α, and β increased. Also an empirical equation for ΔQ^{-1} as a function of crack damage parameter, ϵ was developed, which was

$$\Delta Q^{-1} = C^1 \ [1-(1-C^2\epsilon)^{C^3}]$$

In order to more completely understand the thermal shock induced damage and the empirical equation developed in this study, further investigation is needed. Further gains in understanding the phenomena of thermal shock of whisker reinforced ceramic composites can be expected from comparing the thermal shock results for composites with thermal shock damage results from monolithic ceramic specimens.

REFERENCES

1. T. Mah, M. G. Mendiratta, A. P. Katz, and K. S. Mazdiyasni, "Recent Developments in Fiber-Reinforced High Temperature Ceramic Composites", Amer. Ceram. Soc. Bull. **66** [2] 304-308, (1987).

2. P. J. Lamicq, G. A. Bernhart, M. M. Dauchin, and J. G. Mace, "SiC/SiC Composite Ceramics", ibid., **65** [2] 336-38 (1986).

3. A. J. Caputo, D. P. Stinton, R. A. Lowden, and T. M. Besman, "Fiber-Reinforced SiC Composites with Improved Mechanical Properties", ibid., **66** [2] 368-72 (1987).

4. L. J. Broutman, Composite Materials Vol. 5-Fracture and Fatigue, Chapter 3, Academic Press, New York, (1974).

5. S. L. Dole, O. Hunter, Jr., F. W. Calderwood, and D. J. Bray, "Microcracing of Monoclinic HfO_2", J. Amer. Ceram. Soc., **61**; 486-72 (1978)

6. E. Bonetti, E. Evangelista, and P. Gondi, "High Temperature Damping in Si_3N_4 Depending on the Sintering Conditions", Internal Friction and Ultrasonic Attenuation in Solids, 401-405, Pergamon Press, New York, (1980).

7. S. L. Dole, O. Hunter, Jr., and C. J. Wooge, "Elastic Properties of Monoclinic Hafnium Oxide at Room Temperature", J. Amer. Ceram. Soc. **60** [11-12] 488-90 (1977).

8. C. J. Malarky, "Effects of Microstructure on the Elastic Properties of Selected Ta_2O_5-Eu_2O_3 Compositions", M. S. Thesis, Iowa State University, 43-44 (1977).

9. K. Matsushita, S. Kuratani, T. Okamoto and M. Shimada, "Young's Modulus and Internal Friction in Alumina Subjected to Thermal Shock", J. Mat. Sci. Lett., 3 345-48 (1984).

10. S. L. Dole, O. Hunter, Jr., "Elastic Properties of Hafnium and Zirconium Oxides Stabilized with Praseodium or Terbium Oxide", J. Amer. Ceram. Soc., **66** [3] C-47-C-49 (1983).

11. Eighth International Conference on Internal Friction and Ultrasonic Attenuation in Solids, University of Illinois, J. de Physique, Colloque, ISSN, C10-427-C10-493, no.10, (1985).

12. Fourth European Conference on Internal Friction and Ultrasonic Attenuation in Solids, Villeurbanne, France, J. de Physique, Colloque, ISSN, C9-85-C9-203, no.9, (1983).

13. A. S. Nowick, B. S. Berry, Anelastic Relaxation in Crystalline Solids, Chapter 1, Academic Press, New York, (1972).

14. J. B. Wachtman, Jr., and W. E. Tefft, "Effect of Suspension Position on Apparant Values of Internal Friction Determined by Forster's Method ", Rev. Sci. Instrs., 29 [6] 517-20 (1958).

15. C. Zener, Elasticity and Anelasticity of Metals, University of Chicago Press, Chicago, p.60, (1948).

16. F. Forster, "A New Method for the Determination of the Modulus of Elasticity and Damping", Zeit. Metallkunde, 29 [4] 109-15 (1937).

17. E. Schreiber, O. L. Anderson, and N. Soga, Elastic Constants and Their Measurement, Chapter 4, McGraw-Hill, New York, (1974).

18. G. Pickett, "Equations for Computing Elastic Constants from Flexural and Torsional Resonant Frequencies of Vibration of Prisms and Cylinders", ASTM Proc., 45, 846-65, (1945).

19. D. P. H. Hasselman, Tables for the Computation of Shear Modulus and Young's Modulus of Elasticity from Resonant Frequencies of Rectangular Prisms, Camborundum Co., Niagara Falls, New York, (1961).

20. L. Rayleigh, The Theory of Sound, Dover Publications, New York, Vol.1, pp. 253-83, (1945).

21. M. A. Meyer and K. K. Chawla, Mechanical Metallurgy - Principles and Applications, Prentice-Hall, p.458, (1984).

22. H. M. Ledbetter, "Dynamic Elastic Modulus and Internal Friction in Fibrous Composites", Nonmetallic Materials and Composites at Low Temperatures, Plenum, New York, pp. 267-81, (1979).

23. P. S. Chau, "Characterization of the Interfacial Adhesion Using Tan Delta", Sampe Quarterly, 19 [1] 10-15 (1987).

24. W. R. Manning and O. Hunter, Jr., "Elastic Properties of Polycrystalline Yttrium Oxide, Holumium Oxide, and Erbium Oxide; High-Temperature Measurements", J. Amer. Ceram. Sco., 52 [9] 492-96 (1969).

25. J. A. Haglund and O. Hunter, Jr., "Elastic Properties of Polycrystalline Monoclinic Gd_2O_3", Ibid., 55 [6] 327-30 (1973).

26. E. D. Case, J. G. Smyth, and O. Hunter, Jr., Fracture Mechanics of Ceramics-Vol. 5, pp. 507-30, edited by R. C. Bradt, A. G. Evans, D. P. H. Hasselman, and F. F. Lange, Plenum Press, New York, (1983).

27. J. A. Coppola and R. C. Bradt, "Thermal-Shock Damage in SiC", Ibid., 56 [4] 214-218 (1973).

28. B. Budiansky and R. J. O'Connell, "Elastic Moduli of a Cracked Solid ", Int. J. Solids Structures 12 81-97 (1975).

29. R. L. Salganik, Mech. Solids 8 [4] 135 (1973); English Translation.